Trapped Modes near Venice Storm Gates

by

Ching-Yi Liao

Submitted to the Department of Civil and Environmental Engineering
in partial fulfillment of the requirements for the degree of

Master of Science in Civil and Environmental Engineering

at the

MASSACHUSETTS INSTITUTE OF TECHNOLOGY

June 1999

Author .....
Department of Civil and Environmental Engineering
May 7, 1999

Certified by .....
Chiang C. Mei
E. K. Turner Professor of Civil and Environmental Engineering
Thesis Supervisor

Accepted by .....
Andrew J. Whittle
Chairman, Department Committee on Graduate Students

Trapped Modes near Venice Storm Gates

by

Ching-Yi Liao

Submitted to the Department of Civil and Environmental Engineering
on May 7, 1999, in partial fulfillment of the
requirements for the degree of
Master of Science in Civil and Environmental Engineering

Abstract

For protection against storm tides, four mobile barriers, each of which consists of 20 gates hinged at the bottom axis, have been proposed to span the three inlets of the Venice lagoon. In stormy weather these gates are raised from their housing to an inclination of 50° angle, acting as a dam and keeping the water-level difference up to 2 meters across the barrier. The gates were originally expected to swing in unison in response to the normally incident waves, but subsequent laboratory experiments revealed that the neighboring gates can oscillate out-of-phase in a variety of ways and affect the intended efficiency. Extending the linear theory of Mei *et al.*, where trapped waves around vertical rectangular gates are analytically solved, the inclined Venice gates problem is examined here by using the hybrid finite element method, accounting for the sea level differences and local bathymetry. Finite elements are employed only in the immediate neighborhood of the gate, while formal analytical representations are used away from it. Factors affecting the trapped wave period are studied and the results are compared with existing laboratory experiments by Delft Hydraulics Laboratory.

Thesis Supervisor: Chiang C. Mei
Title: E. K. Turner Professor of Civil and Environmental Engineering

Acknowledgments

I would like to take this opportunity to express my gratitude to my advisor, Professor Chiang C. Mei, for his support, guidance, and inspiration. I enjoyed and learned from every meeting and discussion we had. I definitely admire his rich knowledge and experience, as well as all his passion toward life and research.

I am also grateful to all the people in my group, and friends who have been there for me for the past two years. Jie, Zhenhua, Chin, Yo-Ming, Yi-San, Jung-Chi and Dr. Su, thanks for your 'technical support'. Pei-Ting, Ching-Yin, Woman, Bruce, Maria, Chia-Chin, Maisie, Flora, Karen, Shou-Yi, Andrew, Gilbert, Ching-Yi, Clare and Yuan ...I'll always remember how we shared our thoughts, our minds and our hearts!!

I appreciate the financial support by Office of Naval Research (Grant N00014-92-J-1754 directed by Dr. Thomas Swean) and National Science Foundation (Grant CTS 9634120, directed by Dr. Roger Arndt). The experimental data are taken from reports provided by Ing. Alberto Scotti and Ing. Yuil Eprim of Technital, Milan, and by Ing. Maria Teresa Brotto of Consorzio Venezia Nuova. My earnest thanks to them.

And, finally, Pa and Mom, thanks for being wonderfully supportive. Yes, I made it!

Contents

List of Figures

List of Tables

Chapter 1

Introduction

To protect Venice and nearby islands in the same lagoon from frequent flooding by storm tides from Adriatic Sea, Consorzio Venezia Nuova has been planning a design of four mobile barriers to span the three inlets of the Venice lagoon, with one across Chiogia and Malamocco inlets and two across Lido inlet where an artificial island separates two barriers. Each barrier consists of 20 gates hinged at the bottom along a fixed axis spanning the inlet, as shown in Figure 1-1. Each gate is a hollow steel box of 20 m length and 4 to 5 m thickness. The height varies from 15 to 25 m depending on the inlet depth. In calm weather all gates are lowered by filling the boxes with water to their housings on the seabed to allow normal navigation. When a storm is imminent, the gates are raised to a 50 degree inclination, by injecting compressed air to expel water, so that the water-level difference up to 2 meters can be maintained.

The designed gates are unconnected for easy manufacturing, installation and maintenance, and were originally expected to swing in unison under normally incident waves. Subsequent laboratory experiments for monochromatic waves, however, revealed that the neighboring gates can oscillate out-of-phase in a variety of ways, producing openings between them and affect the intended efficiency as a dam (Consorzio Venezia Nuova [12]; Varisco [19]). The gate oscillations were found to occur at a period that is twice that of the incoming wave and with relatively large amplitude. Many experiments have been carried out for various dimensions of the same design; these experiments have only been documented in internal reports by Consorzio

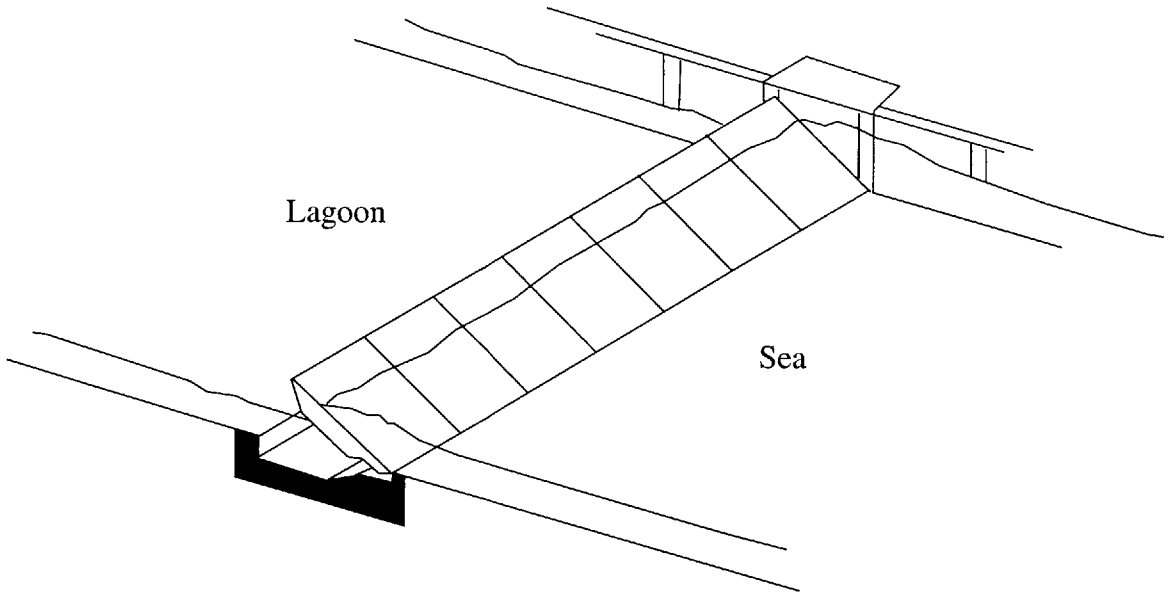

Figure 1-1: Sketch of the mobile barrier.

Venezia Nuova [12].

This phenomenon of *subharmonic resonance* has later been studied theoretically by Blondeaux *et al.* [1][2] and Vittori *et al.* [22] who treated a simplified model under the following assumptions: (i) waves are much longer than the water depth; (ii) the gates are modeled as plane vertical plates sliding along the bottom; (iii) the buoyancy restoring force is replaced by a spring; and (iv) the length of the gates is so small that the barrier moves like a continuous surface (Vittori [20][21]). Mei *et al.* [9] studied a more realistic geometry where the gates are of finite dimensions. To enable analytical computations the gates were assumed to be rectangular boxes standing vertically at static equilibrium. The difference in water levels between the sea and the lagoon was not considered. The natural modes of trapped waves for the water/gate system were deduced by a linear theory and checked by laboratory experiments. Sammarco *et al.* [14][15] further described how these natural modes can be resonated by incident waves through a nonlinear mechanism. For both monochromatic and bi-harmonic incident waves, nonlinear bifurcations including chaos have been examined theoretically and confirmed experimentally [13].

In the proposed design, the operating gates are inclined at the average angle of 50° from the horizon. Since design by model experiments can be conclusive only if all the parameters are varied over a wide range, at the expense of long time and high cost, it is useful to construct a mathematical model to guide the design process. In light of the investigations carried out for vertical gates, a comprehensive model must consist of at least two parts. In the first, one must predict the resonance frequencies for a given gate geometry accounting for the sea level differences and local bathymetry; this is a linearized problem. In the second, one must predict the gate motion at resonance forced by incident waves with a wide variety of spectra; this is a nonlinear problem. Here we shall examine the first (linear) problem. The eigen-modes of trapped waves will be computed by the numerical method of hybrid elements so that finite elements are employed only in the immediate neighborhood of the gate, and the formal analytical solution is used away from it. A general numerical program is constructed so that arbitrary gate geometry, variable bathymetry, and water level difference across the barrier are all considered. As a check, the simplified case where the gates are vertical and rectangular is solved numerically and compared with the analytical solution of Mei *et al.* [9]. The same simplified model, assuming rectangular yet inclined gates, was also tested. Finally, using the prototype design, the role of the gate geometry on the eigen-period is examined and the results are compared with existing laboratory experiments by Delft Hydraulics Laboratory [12]. These results can be possible reference in the final design. The nonlinear problem of subharmonic resonance by incident wave will be left for a future study.

Chapter 2

Problem formulation

Figure 2-1 shows two typical modes of the gate motion in a top view. Since the mobile gates are inclined from the horizon, the mean position of the top of the gates in general does not coincide with y-axis, where the gates are hinged to. These two modes correspond to the most severe reduction of efficiency. In Mode One, every gate moves in opposite phase with its neighbors, *i.e.*, the gate displacements are in the form of $(-+-+\cdots)$ with respect to the mean position. In Mode Two one gate moves backward (or forward) while two neighboring gates move forward (or backward), *i.e.*, the gate displacements are in the form of $(-++-++\cdots)$. Due to periodicity, the analysis can be restricted to one half of the period along the barrier, $0 < y < b$. Thus for Mode One there are two half gates in the half period; for Mode Two, there are one full gate and one half gate in the half period. Higher oscillation modes with longer spatial period in y direction can be found in Sammarco [13] or Mei *et al.* [9], and will not be discussed here.

The typical prototype geometry of the storm gate is shown in Figure 2-2, where the gate is hinged along the sea side edge of its housing at $x = 0$. The walls of the gate are

$$x = \xi^+(z,t) \quad x = \xi^-(z,t)$$

The instantaneous and static angles of inclinations are Θ and $\bar{\Theta}$ from the horizon

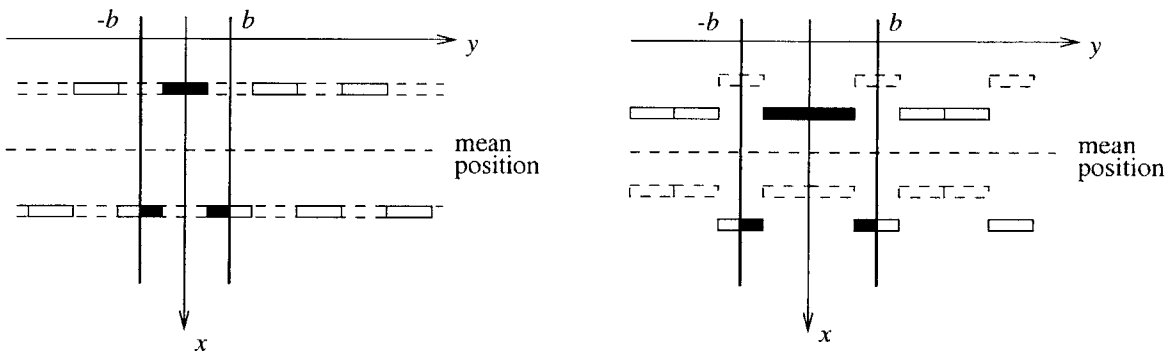

a) MODE 1 b) MODE 2

Figure 2-1: First two modes of possible model responses.

respectively, *i.e.*,

$$\Theta = \bar{\Theta} + \theta(y,t) \tag{2.1}$$

with the dynamic angular displacement θ taking different values for gates I and II in the half period,

$$\theta(y,t) = \begin{cases} \theta^I, & 0 < y < (1-r)b \\ \theta^{II}, & (1-r)b < y < b \end{cases}$$

with $r = 1/2$ and $r = 1/3$ for Modes One and Two, respectively. The lagoon side of the gate is distinguished by the superscript $+$ while the sea side by the superscript $-$. The water depths on two sides are denoted by h^+ and h^-, which are functions of x. The $x \sim y$ plane is chosen to lie on the free surface, *i.e.*, $z = 0$. When sea levels across the barrier are different, the z-coordinate will be defined accordingly for either side. As shown in Figure 2-2, the origins of x- and z-axis will be located differently, *i.e.*, O^+ for the lagoon side while O^- for the sea side. Strictly speaking we should use (x^+, z^+) and (x^-, z^-) for the coordinates, since they are generally different. But the same symbols will be used for simplicity. Viscous forces and friction on the hinges are not considered.

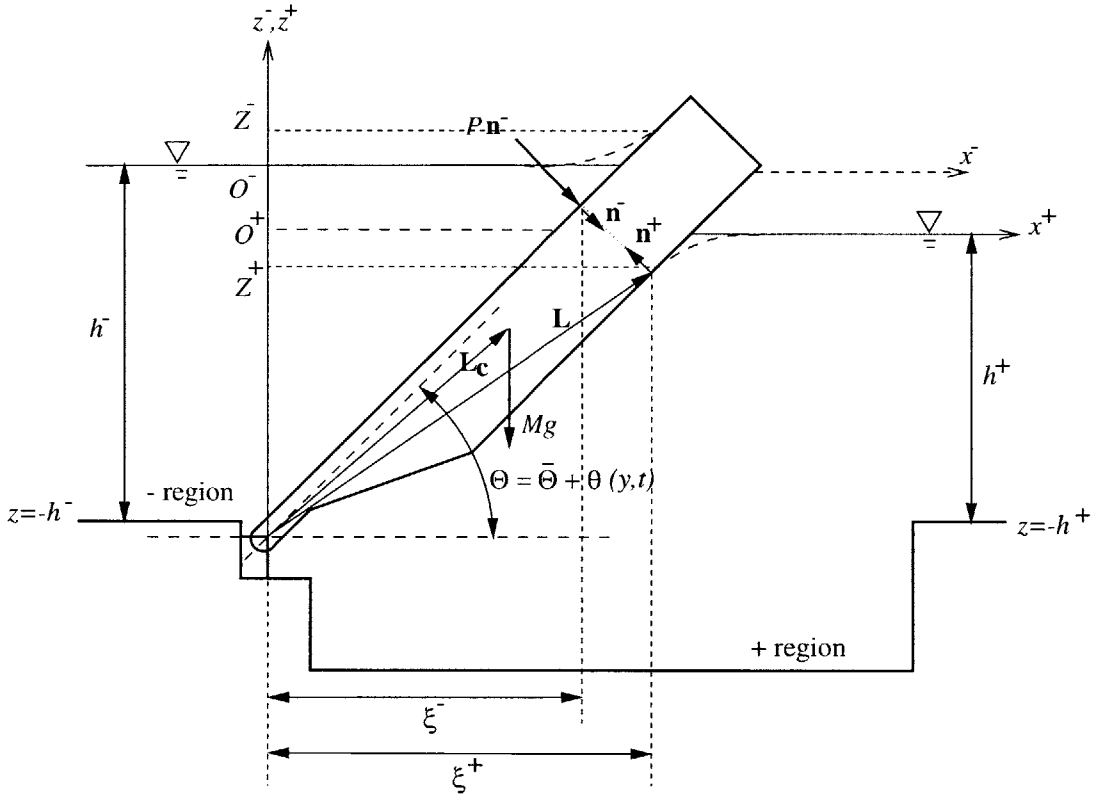

Figure 2-2: Prototype geometry and notations.

2.1 Governing equations

The velocity potential ϕ is governed by:

$$\nabla^2\phi = 0 \tag{2.2}$$

Let the material derivative be denoted by

$$\frac{d}{dt} \equiv \frac{\partial}{\partial t} + \mathbf{u} \cdot \nabla$$

then the kinematic boundary conditions are:

$$\frac{d}{dt}(z - \zeta) = 0 \tag{2.3}$$

on the unknown free surface $z = \zeta(x, y, t)$,

$$\frac{d}{dt}(z + h^{\pm}) = 0 \tag{2.4}$$

on the sea bottom $z = -h^{\pm}(x)$, and

$$\frac{d}{dt}\left(x - \xi^{\pm}\right) = 0 \tag{2.5}$$

on the front and back walls of the gate $x = \xi^{\pm}(z, t)$. On the planes of symmetry in a spatial period, we have

$$\frac{\partial\phi}{\partial y} = 0 \quad y = 0,\ y = b. \tag{2.6}$$

In addition, the potential diminishes to zero when x approaches $\pm\infty$.

Using g for gravitational acceleration, P for pressure and ρ for fluid density, Bernoulli equation gives

$$P = -\rho g z - \rho\frac{\partial\phi}{\partial t} - \frac{1}{2}\rho|\nabla\phi|^2 \tag{2.7}$$

On the free surface, the dynamic condition of uniform atmospheric pressure reads

$$\zeta = -\frac{1}{g}\frac{\partial \phi}{\partial t} - \frac{1}{2g}|\nabla \phi|^2 \tag{2.8}$$

where ζ is an unknown function of (x, y, t).

Eq. (2.3) and (2.8) can be combined to give

$$g\frac{\partial \phi}{\partial z} + \frac{\partial^2 \phi}{\partial z^2} + \frac{\partial}{\partial t}|\nabla \phi|^2 + \frac{1}{2}\nabla \phi \cdot \nabla |\nabla \phi|^2 = 0 \quad z = \zeta \tag{2.9}$$

on the free surface. On the seabed we have

$$\phi_z = -\phi_x h_x^{\pm} \quad i.e. \quad \frac{\partial \phi}{\partial n} = 0 \tag{2.10}$$

at $z = -h^{\pm}(x)$. Let us define the gate rotation vector as $-\Theta \mathbf{e_2}$, where $\mathbf{e_2}$ is the unit vector in y direction. A minus sign is introduced since the positive y-axis points into the paper and counter-clockwise rotation with respect to negative y-axis is regarded as positive Θ here. From eq. (2.5), we have

$$\frac{\partial \phi}{\partial n} = -\frac{d\Theta}{dt}\mathbf{e_2} \cdot (\mathbf{L} \times \mathbf{n}) \tag{2.11}$$

on the gate walls $x = \xi^{\pm}(z, t)$, where $\mathbf{n}$ is the unit normal vector pointing into the gate.

Now we consider the dynamics of either gate I or gate II. Conservation of angular momentum gives

$$-I\frac{d^2\Theta}{dt^2}\mathbf{e_2} = \mathbf{T_g} + \mathbf{T_p} \tag{2.12}$$

where

$$I = I_{xx} + I_{zz} \tag{2.13}$$

is the moment of inertia of the gate about the bottom axis. Torques are defined to be positive if clockwise, *i.e.*, rotating with respect to the positive y-axis. $\mathbf{T_g}$ denotes

the torque due to the weight of the gate,

$$\mathbf{T_g} = \mathbf{L_c} \times (-Mg\mathbf{e_3}) \tag{2.14}$$

with M being the total mass, and $\mathbf{L_c}$ the position vector of the center of gravity of the gate from the hinge. $\mathbf{T_p}$ is the buoyancy torque exerted by the fluid on both sides of the gate

$$\mathbf{T_p} = \mathbf{T_p}^- + \mathbf{T_p}^+ \tag{2.15}$$

As shown in Figure 2-2, $\mathbf{T_p}^-$ is due to fluid pressure from the sea side,

$$\mathbf{T_p}^- = \iint_{S^-} \left(\mathbf{L} \times P\mathbf{n}^-\right) dS \tag{2.16}$$

where the surface integration is performed along the gate contour S^- under the water surface. Similarly, $\mathbf{T_p}^+$ is induced by fluid pressure from the lagoon side. Eq. (2.12) then becomes

$$\begin{aligned} -I\frac{d^2\Theta}{dt^2}\mathbf{e_2} &= \mathbf{L_c} \times (-Mg\mathbf{e_3}) \\ &+ \int_\Lambda \int_{z=-h^-(0)}^{Z^-} \left(\mathbf{L} \times P\mathbf{n}^-\right) \frac{ds}{dz}\, dy\, dz + \int_\Lambda \int_{z=-h^+(0)}^{Z^+} \left(\mathbf{L} \times P\mathbf{n}^+\right) \frac{ds}{dz}\, dy\, dz \end{aligned} \tag{2.17}$$

The integration domain Λ of y is $(0, (1-r)b)$ for gate I and $((1-r)b, b)$ for gate II. ds is the elemental arc length along the gate contour in a vertical $x \sim z$ plane, therefore the factor ds/dz is introduced for the change of variable from s to z. In the z direction, we integrate from $-h^{\pm}(0)$, which denotes the z-coordinate of the hinge, to $Z^{\pm}$ which is the free surface height along either side of the gate-wall,

$$Z^{\pm} = \zeta^{\pm}(x = \xi^{\pm}, y, t) \tag{2.18}$$

as shown in Figure 2-2. In principle the pressure P can be obtained from eq.(2.7).

2.2 Normalization

The equations in the preceding section can be normalized in the following manner, where primes denote dimensionless quantities:

$$\mathbf{x}' = \mathbf{x}/b,\ \mathbf{L}' = \mathbf{L}/b,\ t' = \omega t,\ \phi' = \frac{\phi}{A\omega b},\ \zeta' = \zeta/A,\ h'^{\pm} = h^{\pm}/b$$

Here ω is the natural frequency of the gate, and A is the amplitude of wave motion. The water depth $h^{\pm}$ is assumed to be of the same order of magnitude of b, which is one half of the spatial period in y direction.

As a measurement of small parameter, we introduce

$$\epsilon = \frac{A}{b} \tag{2.19}$$

Recall that in eq. (2.1), $\theta(y,t)$ is the angular displacement of the gate from the mean position which should be of the order of $O(\epsilon)$. We normalize the angular displacement by

$$\theta' = \frac{\Theta - \bar{\Theta}}{\epsilon} = \frac{\theta}{\epsilon}$$

In normalized variables distinguished by primes, eq. (2.2) becomes

$$\nabla'^2\phi' = 0 \tag{2.20}$$

The free surface condition (2.9) becomes

$$G\frac{\partial\phi'}{\partial z'} + \frac{\partial^2\phi'}{\partial t'^2} + \epsilon\frac{\partial}{\partial t'}|\nabla'\phi'|^2 + \frac{1}{2}\epsilon^2\nabla'\phi'\cdot\nabla'|\nabla'\phi'|^2 = 0 \tag{2.21}$$

on $z' = \epsilon\zeta'$, where $G = g/\omega^2 b$. On the sea bottom we have

$$\frac{\partial\phi'}{\partial n} = 0 \tag{2.22}$$

on $z' = -h'^{\pm}(x')$. On the gate walls we have

$$\frac{\partial \phi'}{\partial n} = -\frac{d\theta'}{dt'}\mathbf{e_2} \cdot (\mathbf{L}' \times \mathbf{n}) \tag{2.23}$$

on $x' = \xi'^{\pm}(z', t')$, with the rotation vector defined as $-\epsilon\theta'\mathbf{e_2}$. The dynamic condition eq. (2.17) becomes

$$\begin{aligned} -\epsilon\frac{I}{\rho b^5}\frac{d^2\theta'}{dt'^2}\mathbf{e_2} &= -\frac{M}{\rho b^3}\, G\, (\mathbf{L_c}' \times \mathbf{e_3}) \\ &+ \int_{\Lambda'} dy' \int_{z'=-h'^-(0)}^{\epsilon\zeta'^-} \left[\left(-Gz' - \epsilon\frac{\partial \phi'^-}{\partial t'} - \frac{1}{2}\epsilon^2|\nabla'\phi'^-|^2\right)\left(\mathbf{L}' \times \mathbf{n}^-\right)\right]\frac{ds'}{dz'}\, dz' \\ &+ \int_{\Lambda'} dy' \int_{z'=-h'^+(0)}^{\epsilon\zeta'^+} \left[\left(-Gz' - \epsilon\frac{\partial \phi'^+}{\partial t'} - \frac{1}{2}\epsilon^2|\nabla'\phi'^+|^2\right)\left(\mathbf{L}' \times \mathbf{n}^+\right)\right]\frac{ds'}{dz'}\, dz' \end{aligned} \tag{2.24}$$

where the normalized Bernoulli equation

$$\frac{P}{\rho b^2\omega^2} = -Gz' - \epsilon\frac{\partial \phi'}{\partial t'} - \frac{1}{2}\epsilon^2|\nabla'\phi'|^2 \tag{2.25}$$

has been applied.

2.3 Linearization

For $\epsilon \ll 1$ the free surface boundary condition is linearized to

$$G\frac{\partial \phi'}{\partial z'} + \frac{\partial^2 \phi'}{\partial t'^2} = 0 \tag{2.26}$$

at $z' = 0$. On the walls of the gate, we have to the first order,

$$\mathbf{L}'|_{x'=\xi'^{\pm}} = \bar{\mathbf{L}}'|_{x'=\bar{\xi}'^{\pm}} + \epsilon\left(-\theta'\mathbf{e_2} \times \bar{\mathbf{L}}'\right)_{x'=\bar{\xi}'^{\pm}} \tag{2.27}$$

Here $\bar{\mathbf{L}}'$ is the dimensionless position vector of a point on the static gate surface $x' = \bar{\xi}'^{\pm}$. The kinematic boundary condition (2.23) becomes, to the first order,

$$\frac{\partial \phi'}{\partial \bar{n}^{\pm}} = -\frac{d\theta'}{dt'}\mathbf{e_2} \cdot \left(\bar{\mathbf{L}}' \times \bar{\mathbf{n}}^{\pm}\right) \tag{2.28}$$

at $x' = \bar{\xi}'^{\pm}(z')$, where $\bar{\mathbf{n}}^{\pm}$ is the unit normal vector pointing into the gate at the mean position.

Let us now linearize the dynamic boundary condition. By using eq. (2.27) and the vector identity

$$(\mathbf{a} \times \mathbf{b}) \times \mathbf{c} = (\mathbf{a} \cdot \mathbf{c})\mathbf{b} - (\mathbf{b} \cdot \mathbf{c})\mathbf{a} \tag{2.29}$$

in eq. (2.24), we find,

$$\begin{aligned} \mathbf{L}' \times \mathbf{n} &= \left[\bar{\mathbf{L}}' + \epsilon(-\theta'\mathbf{e_2} \times \bar{\mathbf{L}}')\right] \times [\bar{\mathbf{n}} + \epsilon(-\theta'\mathbf{e_2} \times \bar{\mathbf{n}})] \\ &= \bar{\mathbf{L}}' \times \bar{\mathbf{n}} - \epsilon\theta' \left[(\mathbf{e_2} \times \bar{\mathbf{L}}') \times \bar{\mathbf{n}} + \bar{\mathbf{L}}' \times (\mathbf{e_2} \times \bar{\mathbf{n}})\right] \\ &= \bar{\mathbf{L}}' \times \bar{\mathbf{n}} \end{aligned} \tag{2.30}$$

i.e., the moment arm of the pressure force acting at a fixed point on the gate walls remains unchanged by the motion of rotation. Keeping terms up to $O(\epsilon)$, we have, from eq. (2.24):

$$\begin{aligned} -\epsilon\frac{I}{\rho b^5}\frac{d^2\theta'}{dt'^2}\mathbf{e_2} = &-\frac{M}{\rho b^3} G \left(\bar{\mathbf{L}_\mathbf{c}}' \times \mathbf{e_3}\right) - \frac{M}{\rho b^3} G\epsilon \left(-\theta'\mathbf{e_2} \times \bar{\mathbf{L}_\mathbf{c}}'\right) \times \mathbf{e_3} \\ &- \left\{ \int_{\Lambda'} dy' \times \left[\int_{z'=-h'^-(0)}^{\epsilon\zeta'^-} \left(G(\mathbf{L}' \cdot \mathbf{e_3} - h'^-(0)) + \epsilon\frac{\partial\phi'^-}{\partial t'} \right) \left(\bar{\mathbf{L}}' \times \bar{\mathbf{n}}^-\right) \frac{ds'}{dz'} dz' \right.\right. \\ &\left.\left. + \int_{z'=-h'^+(0)}^{\epsilon\zeta'^+} \left(G(\mathbf{L}' \cdot \mathbf{e_3} - h'^+(0)) + \epsilon\frac{\partial\phi'^+}{\partial t'} \right) \left(\bar{\mathbf{L}}' \times \bar{\mathbf{n}}^+\right) \frac{ds'}{dz'} dz' \right] \right\} \end{aligned} \tag{2.31}$$

where we have expressed the vertical coordinate of a point on the gate surface by

$$z' = \mathbf{L}' \cdot \mathbf{e_3} - h'^{\pm}(0)$$

After some algebra, we find from eq. (2.31) that at the order $O(\epsilon^0)$:

$$\begin{aligned} 0 &= \frac{M}{\rho b^3} G \left(\bar{\mathbf{L}_\mathbf{c}}' \times \mathbf{e_3}\right) \\ &+ \int_{\Lambda'} dy' \times \left[\int_{\bar{z}'=-h'^-(0)}^{0} G\bar{z}' \left(\bar{\mathbf{L}}' \times \bar{\mathbf{n}}^-\right) \frac{ds'}{dz'} dz' + \int_{\bar{z}'=-h'^+(0)}^{0} G\bar{z}' \left(\bar{\mathbf{L}}' \times \bar{\mathbf{n}}^+\right) \frac{ds'}{dz'} dz' \right] \end{aligned} \tag{2.32}$$

in which

$$\bar{z}' = \bar{\mathbf{L}}' \cdot \mathbf{e_3} - h'^{\pm}(0)$$

denotes the z-coordinate of a point on the gate walls at mean position. This condition describes the static equilibrium between the static gravity torque $\mathbf{T_g}$ (the first term) and the static buoyancy torque (the integrals), which can be found for a given equilibrium angle $\bar{\Theta}$. The geometry and total mass of the gate can be chosen to achieve the desired mean inclination angle.

Since the value of the integral over the vertical interval from $z' = 0$ to $z' = \epsilon\zeta'^{\pm}$ is small

$$\int_{z'=0}^{\epsilon\zeta'^{\pm}} Gz' \left(\bar{\mathbf{L}}' \times \bar{\mathbf{n}}^{\pm}\right) \frac{ds'}{dz'} dz' = O(z'^2) = O(\epsilon^2)$$

we have, at the order $O(\epsilon)$,

$$\begin{aligned}
\frac{I}{\rho b^5}\frac{d^2\theta'}{dt'^2}\mathbf{e_2} = &-\frac{M}{\rho b^3} G\theta' \left(\mathbf{e_2} \times \bar{\mathbf{L}_c}'\right) \times \mathbf{e_3} \\
&+ \left\{ \int_{\Lambda'} dy' \times \left[\int_{\bar{z}'=-h'^-(0)}^{0} \left(\frac{\partial \phi'^-}{\partial t'} - G\theta'(\mathbf{e_2} \times \bar{\mathbf{L}}') \cdot \mathbf{e_3} \right) (\bar{\mathbf{L}}' \times \bar{\mathbf{n}}^-) \frac{ds'}{dz'} dz' \right.\right. \\
&\left.\left. + \int_{\bar{z}'=-h'^+(0)}^{0} \left(\frac{\partial \phi'^+}{\partial t'} - G\theta'(\mathbf{e_2} \times \bar{\mathbf{L}}') \cdot \mathbf{e_3} \right) (\bar{\mathbf{L}}' \times \bar{\mathbf{n}}^+) \frac{ds'}{dz'} dz' \right] \right\}
\end{aligned} \tag{2.33}$$

where the integration domain is the gate surface at equilibrium position.

2.4 Summary of linearized governing equations

Returning to physical quantities, the linearized governing equations are

$$\nabla^2 \phi = 0 \tag{2.34}$$

in the fluid,

$$g\frac{\partial \phi}{\partial z} + \frac{\partial^2 \phi}{\partial t^2} = 0 \tag{2.35}$$

at $z = 0$,

$$\frac{\partial \phi}{\partial n} = 0 \tag{2.36}$$

at $z = -h^{\pm}(x)$, and

$$\frac{\partial \phi}{\partial \bar{n}^{\pm}} = \pm \frac{A}{b} \frac{d\theta'}{dt} |\bar{\mathbf{L}} \times \bar{\mathbf{n}}^{\pm}| \tag{2.37}$$

at $x = \bar{\xi}^{\pm}(z)$. Since

$$(\mathbf{e_2} \times \bar{\mathbf{L}}) \cdot \mathbf{e_3} = (\bar{\mathbf{L}} \times \mathbf{e_3}) \cdot \mathbf{e_2} = -\bar{\xi}(z)$$

on the walls of the gate, the y-component of eq. (2.33) becomes

$$\begin{aligned} I\frac{d^2\theta'}{dt^2} &= Mg\theta'(\bar{\mathbf{L}}_{\mathbf{c}} \cdot \mathbf{e_3}) \\ &+ \left\{ \int_{\Lambda} dy \times \left[\int_{\bar{z}=-h^-(0)}^{0} \left(\rho \frac{\partial \phi^-}{\partial t} + \rho g \theta' \bar{\xi}^-(z) \right) |\bar{\mathbf{L}} \times \bar{\mathbf{n}}^-| \frac{ds}{dz} dz \right. \right. \\ &\left. \left. - \int_{\bar{z}=-h^+(0)}^{0} \left(\rho \frac{\partial \phi^+}{\partial t} + \rho g \theta' \bar{\xi}^+(z) \right) |\bar{\mathbf{L}} \times \bar{\mathbf{n}}^+| \frac{ds}{dz} dz \right] \right\} \end{aligned} \tag{2.38}$$

with the static equilibrium condition,

$$\begin{aligned} 0 = &-Mg|\bar{\mathbf{L}}_{\mathbf{c}} \times \mathbf{e_3}| + \int_{\Lambda} dy \times \\ &\left[\int_{\bar{z}=-h^-(0)}^{0} \rho g \bar{z} |\bar{\mathbf{L}} \times \bar{\mathbf{n}}^-| \frac{ds}{dz} dz - \int_{\bar{z}=-h^+(0)}^{0} \rho g \bar{z} |\bar{\mathbf{L}} \times \bar{\mathbf{n}}^+| \frac{ds}{dz} dz \right] \end{aligned} \tag{2.39}$$

These results are consistent with those known in the dynamics of two dimensional floating bodies (see *e.g.*, Mei [8], 1989, p 298-300).

2.5 Fourier decomposition in a spatial period

Within the period $-b < y < b$, the gate motion is even in y. We therefore use Fourier cosine series to represent the solution in the half period $0 < y < b$. The wave potential ϕ can be described as

$$\phi = \sum_{m=1}^{\infty} M_m \cos\left(\frac{m\pi y}{b}\right) e^{-i\omega t} + * \tag{2.40}$$

where $*$ denotes the complex conjugate of the preceding term. Following Mei *et al.* [9], the gate motion is represented by

$$\theta' = \frac{b}{A}\theta(y)e^{-i\omega t} + * \tag{2.41}$$

To ensure the absence of the long-crested propagating wave, we require that

$$\int_{-b}^{b} \theta(y)dy = 0 \tag{2.42}$$

thus

$$\theta^{II} = \theta^{I}\left(\frac{1-r}{r}\right) \tag{2.43}$$

Then θ' can be derived as

$$\theta' = \frac{b}{A}\theta^{I}\sum_{m=1}^{\infty} b_m \cos\left(\frac{m\pi y}{b}\right)e^{-i\omega t} + * \tag{2.44}$$

where θ^I is so far arbitrary, and

$$b_m = \frac{2}{m\pi r}\sin m\pi(1-r) \tag{2.45}$$

are known real coefficients. The linearized governing equations of $M_m^{\pm}$ can be derived from eq. (2.34) through eq. (2.39):

$$\frac{\partial^2 M_m^{\pm}}{\partial x^2} + \frac{\partial^2 M_m^{\pm}}{\partial z^2} = \left(\frac{m\pi}{b}\right)^2 M_m^{\pm} \tag{2.46}$$

in the fluid,

$$\frac{\partial M_m^{\pm}}{\partial z} - \frac{\omega^2}{g}M_m^{\pm} = 0 \tag{2.47}$$

at $z = 0$,

$$\frac{\partial M_m^{\pm}}{\partial n} = 0 \tag{2.48}$$

at $z = -h^{\pm}(x)$, and

$$\frac{\partial M_m^{\pm}}{\partial \bar{n}^{\pm}} = \mp i\omega\theta^I b_m |\bar{\mathbf{L}} \times \bar{\mathbf{n}}^{\pm}| \tag{2.49}$$

at $x = \bar{\xi}^{\pm}(z)$. Note that $M_m^{\pm}$ and θ^I are out of phase by 90°. Consider gate I in $0 < y < b(1-r)$, *i.e.*, the half gate for Mode One and the full gate for Mode Two, the dynamic condition of the gate motion eq.(2.38) gives the eigen value condition for ω:

$$\omega^2 \left(I + I_a(\omega)\right) = C \tag{2.50}$$

where

$$\begin{aligned} I_a(\omega) &= \frac{i\rho}{\omega\theta^I} \sum_{m=1}^{\infty} \int_0^{(1-r)b} \cos\left(\frac{m\pi y}{b}\right) dy \times \\ &\left[\int_{\bar{z}=-h^-(0)}^{0} M_m^- |\bar{\mathbf{L}} \times \bar{\mathbf{n}}^-| \frac{ds}{dz}\, dz - \int_{\bar{z}=-h^+(0)}^{0} M_m^+ |\bar{\mathbf{L}} \times \bar{\mathbf{n}}^+| \frac{ds}{dz}\, dz\right] \end{aligned} \tag{2.51}$$

is the hydrodynamic moment of inertia, and

$$\begin{aligned} C &= -Mg(\bar{\mathbf{L}}_{\mathbf{c}} \cdot \mathbf{e_3}) \\ &- \rho g \int_0^{(1-r)b} dy \times \left[\int_{\bar{z}=-h^-(0)}^{0} \bar{\xi}^- |\bar{\mathbf{L}} \times \bar{\mathbf{n}}^-| \frac{ds}{dz}\, dz - \int_{\bar{z}=-h^+(0)}^{0} \bar{\xi}^+ |\bar{\mathbf{L}} \times \bar{\mathbf{n}}^+| \frac{ds}{dz}\, dz\right] \end{aligned} \tag{2.52}$$

is the total torque, consisting of torques due to the weight of the gate and the buoyancy restoring force. Since $Mg|\bar{\mathbf{L}}_{\mathbf{c}} \times \mathbf{e_3}|$ can be computed from eq. (2.39), $Mg(\bar{\mathbf{L}}_{\mathbf{c}} \cdot \mathbf{e_3})$ can be found from the inclination of $\bar{\mathbf{L}}_{\mathbf{c}}$. All integrations must be carried out numerically for studying complicated gate geometries.

In view of eq. (2.49), $M_m^{\pm}$ is pure imaginary, thus the dynamic moment of inertia $I_a(\omega)$ is real. Also from eq. (2.49), $M_m^{\pm}$ is proportional to θ^I. Therefore $I_a(\omega)$ is not a function of θ^I. Since C does not depend on θ^I either, the eigen value equation for ω, eq. (2.50), is of course independent of θ^I.

For a given trial value of ω, $M_m^{\pm}$ can be solved for $\theta^I = 1$ from eq. (2.46) through eq. (2.49). If the resulting $I_a(\omega)$ satisfies eq. (2.50), the natural frequency ω of the trapped wave is found. Otherwise iterations are carried out until eq. (2.50) is met.

Chapter 3

Hybrid finite element method

The general idea of *hybrid finite element method* is to use discrete finite elements near the complicated body geometry, and formal analytical representations away from it. In this approach, the boundary value problem for $M_m^{\pm}$ is expressed as a variational principle which incorporates the matching of the finite element region and the analytical region as natural boundary conditions. All the unknowns, including nodal values in the finite element region as well as the expansion coefficients in the analytical region, are solved simultaneously. Continuity of pressure and normal velocity across the imaginary boundary is automatically satisfied in the numerical procedure without iteration. The method is a slightly modified version developed earlier for water wave diffraction and radiation problems, see Yue *et al.* [23] and Mei [8].

3.1 The variational principle

We introduce the imaginary boundaries $x = c^{\pm}$ as shown in Figure 3-1, and let the region Ω between them as the finite element region in which all the complexities of body geometry and bathymetry are confined. In this region the wave potential ϕ is defined in eq. (2.40) where $M_m^{\pm}$ must satisfy eq. (2.46) through eq. (2.49).

Let us define the remaining water region on two sides by $\hat{\Omega}^{\pm}$, where analytical

solutions will be sought. The wave potential here $\hat{\phi}^{\pm}$ is similarly defined as

$$\hat{\phi}^{\pm} = \sum_{m=1}^{\infty} \hat{M}_m^{\pm} \cos\left(\frac{m\pi y}{b}\right) e^{-i\omega t} + * \tag{3.1}$$

and satisfies Laplace equation with out-going boundary conditions. For easy reference, all the analytical variables are distinguished by hats. By assuming constant depth $h^{\pm}$ in $\hat{\Omega}$, the formal analytical solution of $\hat{\phi}$ can be easily derived. Here we adopt the expression from Mei *et al.* [9], that is, in eq.(3.1),

$$\hat{M}_m^{\pm} = \sum_{n=0}^{\infty} \beta_{mn} e^{\mp \alpha_{mn} x} \cosh k_n (z + h^{\pm}) \tag{3.2}$$

where

$$\omega^2 = g k_n \tanh k_n h$$

$$\alpha_{mn} = \sqrt{\left(\frac{m\pi}{b}\right)^2 - k_n^2}$$

k_0 is real, and k_n, n=1, 2, 3, ... are all imaginary quantities corresponding to evanescent modes. The coefficients β_{mn} are yet to be determined. Note that the frequency must be low enough

$$k_0 < \pi/b$$

so that no propagating mode can exist, *i.e.*, the wave is trapped.

The matching conditions across the imaginary boundary between region Ω and $\hat{\Omega}$ are :

$$\phi^{\pm} = \hat{\phi}^{\pm}, \quad \frac{\partial \phi^{\pm}}{\partial x} = \frac{\partial \hat{\phi}^{\pm}}{\partial x} \tag{3.3}$$

Using Fourier cosine series to expand ϕ and $\hat{\phi}$ as in eq. (2.40) and (3.1), the matching between pressure and velocity flux become

$$M_m^{\pm} = \hat{M}_m^{\pm}, \quad \frac{\partial M_m^{\pm}}{\partial x} = \frac{\partial \hat{M}_m^{\pm}}{\partial x} \tag{3.4}$$

at $x = c^{\pm}$.

We shall now prove that, for prescribed V^+, and unit depth in y, the boundary

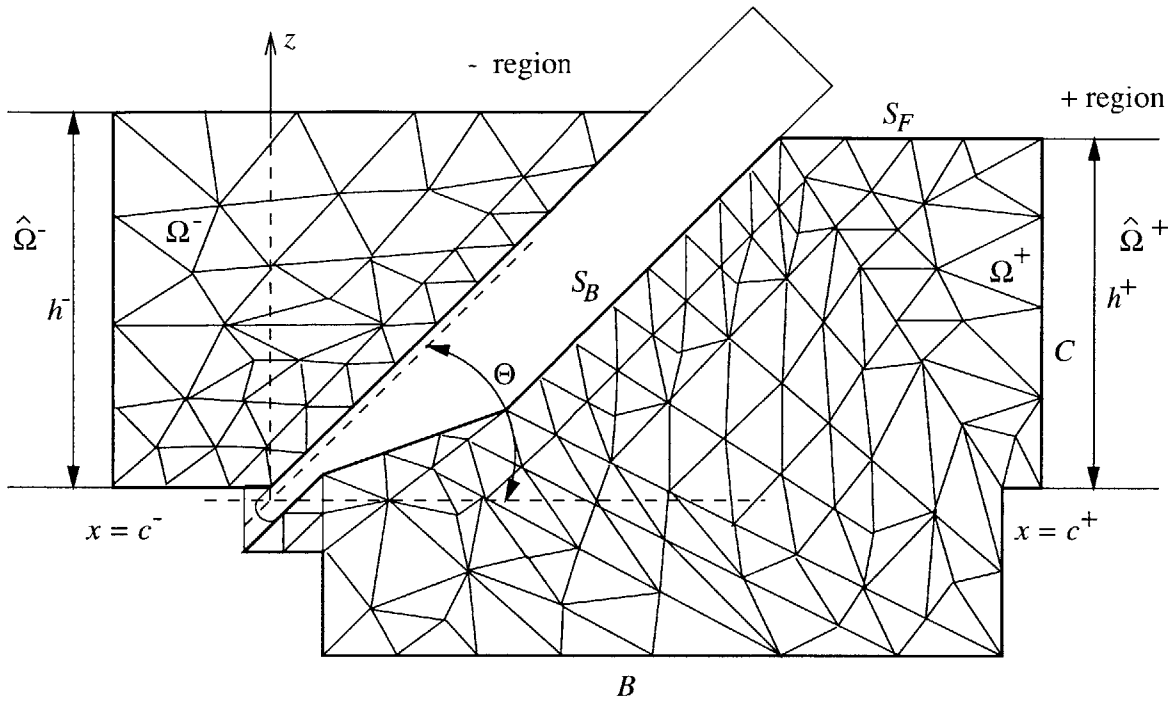

Figure 3-1: Finite element model.

value problem coupling M_m^+ and $\hat{M}_m^+$ is equivalent to the stationarity of the following functional. In the + domain,

$$J^+ = \iint_{\Omega^+} \frac{1}{2}\left[(\nabla M_m^+)^2 + \left(\frac{m\pi}{b}\right)^2 (M_m^+)^2\right] d\Omega - \frac{\omega^2}{2g}\int_{z=0} (M_m^+)^2 dS$$
$$+ \int_{x=c^+} \left(\frac{1}{2}\hat{M}_m^+ - M_m^+\right) \frac{\partial \hat{M}_m^+}{\partial x} dS - \int_{x=\bar{\xi}^+} V^+ M_m^+ \, dS \tag{3.5}$$

where

$$\hat{M}_m^+ = \sum_{n=0}^{\infty} \beta_{mn} e^{-\alpha_{mn} x} \cosh k_n (z + h^+) \tag{3.6}$$

and

$$V^+ = -i\omega b_m |\bar{\mathbf{L}} \times \bar{\mathbf{n}}^+| \tag{3.7}$$

is the normal velocity of the gate on the front wall $x = \bar{\xi}^+$, with θ^I taken to be unity

in eq. (2.49). In the $-$ domain, the functional is

$$J^- = \iint_{\Omega^-} \frac{1}{2}\left[(\nabla M_m^-)^2 + \left(\frac{m\pi}{b}\right)^2 (M_m^-)^2\right] d\Omega - \frac{\omega^2}{2g}\int_{z=0}(M_m^-)^2 dS$$
$$- \int_{x=c^-}\left(\frac{1}{2}\hat{M}_m^- - M_m^-\right)\frac{\partial \hat{M}_m^-}{\partial x} dS - \int_{x=\bar{\xi}^-} V^- M_m^-\, dS \tag{3.8}$$

where

$$\hat{M}_m^- = \sum_{n=0}^{\infty} \beta_{mn} e^{+\alpha_{mn}x} \cosh k_n(z + h^-) \tag{3.9}$$

and

$$V^- = i\omega b_m |\bar{\mathbf{L}} \times \bar{\mathbf{n}}^-| \tag{3.10}$$

is the normal velocity of the gate on the back wall $x = \bar{\xi}^-$.

Hereafter we omit the subscript m for brevity. M, therefore, denotes the mth mode in y direction.

Consider the $+$ region, *i.e.*, the lagoon side. We take the first variation of the functional J^+,

$$\begin{aligned}
\delta J^+ &= \iint_{\Omega^+}\left[\nabla M \cdot \nabla(\delta M) + \left(\frac{m\pi}{b}\right)^2 M\delta M\right] d\Omega \\
&- \frac{\omega^2}{g}\int_{z=0} M\delta M\, dS - \int_{x=\xi^+} V^+\delta M\, dS \\
&+ \int_{x=c^+}\frac{1}{2}(\bar{M} - M)\frac{\partial \delta\hat{M}}{\partial x} dS - \int_{x=c^+}\delta M\frac{\partial \hat{M}}{\partial x}\, dS \\
&+ \int_{x=c^+}\frac{1}{2}\left(\delta\hat{M}\frac{\partial \hat{M}}{\partial x} - \hat{M}\frac{\partial \delta\hat{M}}{\partial x}\right) dS
\end{aligned} \tag{3.11}$$

By applying Green's theorem to $\hat{M}$ and $\delta\hat{M}$ over the region $\hat{\Omega}^+$, the last integral can be shown to vanish identically because both $\hat{M}$ and $\delta\hat{M}$ satisfy Helmholtz equation, identical homogeneous boundary conditions on the free surface and the seabed, and vanish at infinity. We now perform partial integration to the first term of eq. (3.11)

$$\begin{aligned}
&\iint_{\Omega^+}\left[\nabla M \cdot \nabla(\delta M) + \left(\frac{m\pi}{b}\right)^2 M\delta M\right] d\Omega \\
&= \iint_{\Omega^+}\left[\nabla\cdot(\delta M\nabla M) - \delta M\cdot\nabla^2 M + \left(\frac{m\pi}{b}\right)^2 M\delta M\right] d\Omega
\end{aligned}$$

$$= -\iint_{\Omega^+} \left[\nabla^2 M - \left(\frac{m\pi}{b}\right)^2 M\right] \delta M \, d\Omega + \int_{S_F+B+S_B+C} \delta M \frac{\partial M}{\partial n} dS \tag{3.12}$$

Gauss' theorem has been applied thus the second term is the line integral on the boundary of Ω^+ domain, where S_F is along the free surface, B is along the seabed, S_B is on the gate wall $x = \bar{\xi}^+$, and C is the imaginary boundary at $x = c^+$, as shown in Figure 3-1.

After some algebra, eq. (3.11) becomes

$$\begin{aligned}\delta J^+ &= -\iint_{\Omega^+} \left[\nabla^2 M - \left(\frac{m\pi}{b}\right)^2 M\right] \delta M \, d\Omega \\ &+ \int_{S_F} \left(\frac{\partial M}{\partial n} - \frac{\omega^2}{g} M\right) \delta M \, dS + \int_B \frac{\partial M}{\partial n} \delta M \, dS + \int_{S_B} \left(\frac{\partial M}{\partial n} - V^+\right) \delta M \, dS \\ &+ \int_C \left(\frac{\partial M}{\partial n} - \frac{\partial \hat{M}}{\partial n}\right) \delta M \, dS + \int_C \frac{1}{2}(\hat{M} - M) \frac{\partial \delta \hat{M}}{\partial n} dS \end{aligned} \tag{3.13}$$

In order for $\delta J^+ = 0$ for arbitrary δM and $\delta \hat{M}$, M must satisfy Helmholtz equation eq. (2.46), also eq. (2.47) on the free surface S_F, eq. (2.48) on the seabed B, and eq. (2.49) on the gate surface S_B. In addition continuity of M and $\partial M/\partial n$ across the imaginary boundary C are satisfied as *natural boundary conditions.* Therefore, the stationarity of J^+ is equivalent to the boundary value problem coupling M^+ and $\hat{M}^+$. Similar proof can be done for M^- and $\hat{M}^-$ in Ω^-.

Since $\delta \hat{M}$ is arbitrary in the space $C^\infty(\Omega)$, while δM is in the space $H^1(\Omega)$, we restate the variational principle in the *weak form* as follows: For given V^+, find $M \in H^1(\Omega)$ and $\hat{M} \in C^\infty(\Omega)$ such that $\forall \psi \in H^1(\Omega)$,

$$\begin{aligned}&\iint_{\Omega^+} \left[\nabla M \cdot \nabla \psi + \left(\frac{m\pi}{b}\right)^2 M\psi\right] d\Omega \\ &\quad - \frac{\omega^2}{g} \int_{z=0} M\psi \, dS - \int_{x=\bar{\xi}^+} V^+ \psi \, dS - \int_{x=c^+} \psi \frac{\partial \hat{M}}{\partial x} \, dS = 0 \end{aligned} \tag{3.14}$$

and $\forall \hat{\psi} \in C^\infty(\Omega)$,

$$\int_{x=c^+} (\hat{M} - M) \frac{\partial \hat{\psi}}{\partial x} dS = 0 \tag{3.15}$$

Similarly we can find the variational principle in the *weak form* for Ω^- domain.

3.2 Finite element formulation

The finite element region Ω^+ is divided into a triangular network of N_N nodes. If we consider a global shape function $F_i(x_j, z_j) = \delta_{ij}$, which has the value 1 at the node (x_j, z_j), and vanishes at all other nodes, then

$$M = \sum_{i=1}^{N_N} \mu_i F_i(x,z), \quad \psi = \sum_{i=1}^{N_N} \psi_i F_i(x,z) \tag{3.16}$$

where M represents the typical $M_m^{\pm}$, with μ_i and ψ_i being unknown coefficients. In the analytical region $\hat{\Omega}^+$, we express

$$\hat{M} = \sum_{n=0}^{N_T-1} \hat{\beta}_n e^{-\alpha_n x} \cosh k_n(z+h^+), \quad \hat{\psi} = \sum_{n=0}^{N_T-1} \hat{\gamma}_n e^{-\alpha_n x} \cosh k_n(z+h^+) \tag{3.17}$$

where α_n is given in eq. (3.2), $\hat{\beta}_n$, $\hat{\gamma}_n$ are the unknown coefficients. The series are truncated after N_T terms.

The integrals in eq. (3.14) and eq. (3.15) can then be expressed as follows:

$$\begin{aligned} & \iint_{\Omega^+} \left[\nabla M \cdot \nabla \psi + \left(\frac{m\pi}{b}\right)^2 M\psi \right] d\Omega \\ = & \sum_{i=1}^{N_N}\sum_{j=1}^{N_N} \psi_i \left[\iint_{\Omega} \nabla F_j \cdot \nabla F_i + \left(\frac{m\pi}{b}\right)^2 F_j F_i \, d\Omega \right] \mu_j \\ = & \{\psi^+\}^T \left[K_1^+\right] \{\mu^+\}, \end{aligned} \tag{3.18}$$

$$\begin{aligned} -\frac{\omega^2}{g} \int_{z=0} M\psi \, dS &= \sum_{i=1}^{N_F}\sum_{j=1}^{N_F} \psi_i \left[-\frac{\omega^2}{g} \int_{z=0} F_j F_i \, dS \right] \mu_j \\ &= \{\psi^{F^+}\}^T \left[K_2^+\right] \{\mu^{F^+}\} \end{aligned} \tag{3.19}$$

where N_F is the number of nodes on the free surface $z = 0$;

$$\begin{aligned} -\int_{x=\bar{\xi}^+} V^+ \psi \, dS &= -\sum_{i=1}^{N_W^+} \psi_i \left[\int_{x=\xi^+} V^+ F_i \, dS \right] \\ &= -\{\psi^{W^+}\}^T \{V^+\} \end{aligned} \tag{3.20}$$

where N_W^+ is the number of nodes on the gate wall $x = \bar{\xi}^+$;

$$\begin{aligned} -\int_{x=c^+} \psi \frac{\partial \hat{M}}{\partial x} \, dS &= \sum_{i=1}^{N_C^+} \sum_{j=0}^{N_T-1} \psi_i \left[-\int_{x=c^+} -\alpha_j e^{-\alpha_j x} \cosh k_j (z + h^+) F_i \, dS \right] \hat{\beta}_j \\ &= \{\psi^{C^+}\}^T \left[K_3^+ \right] \{\hat{\beta}^+\} \end{aligned} \tag{3.21}$$

where N_C^+ is the number of nodes on the artificial boundary $x = c^+$;

$$\begin{aligned} &\int_{x=c^+} M \frac{\partial \hat{\psi}}{\partial x} \, dS \\ &= \sum_{i=1}^{N_C^+} \sum_{j=0}^{N_T-1} \mu_i \left[\int_{x=c^+} -\alpha_j e^{-\alpha_j x} \cosh k_j (z + h^+) F_i \, dS \right] \hat{\gamma}_j \\ &= -\{\mu^{C^+}\}^T \left[K_3^+ \right] \{\hat{\gamma}^+\} \end{aligned} \tag{3.22}$$

and

$$\begin{aligned} &\int_{x=c^+} \hat{M} \frac{\partial \hat{\psi}}{\partial x} \, dS \\ &= \sum_{i=0}^{N_T-1} \sum_{j=0}^{N_T-1} \hat{\beta}_i \left[\int_{x=c^+} -\alpha_j e^{-\alpha_j x} \cosh k_j (z + h^+) \cdot e^{-\alpha_i x} \cosh k_i (z + h^+) \, dS \right] \hat{\gamma}_j \\ &= \{\hat{\beta}^+\}^T \left[K_4^+ \right] \{\hat{\gamma}^+\} \end{aligned} \tag{3.23}$$

We now collect the integrals and assemble the matrix forms of eq. (3.14) and eq. (3.15) as

$$\begin{aligned} &\{\psi^+\}^T \left[K_1^+ \right] \{\mu^+\} + \{\psi^{F^+}\}^T \left[K_2^+ \right] \{\mu^{F^+}\} \\ &\qquad + \{\psi^{C^+}\}^T \left[K_3^+ \right] \{\hat{\beta}^+\} = \{\psi^{W^+}\}^T \{V^+\} \end{aligned} \tag{3.24}$$

and

$$\{\hat{\gamma}^+\}^T \left[K_3^+\right]^T \{\mu^{C^+}\} + \{\hat{\gamma}^+\}^T \left[K_4^+\right]^T \{\hat{\beta}^+\} = 0 \tag{3.25}$$

Similarly we have in $-$ region

$$\begin{aligned} \{\psi^-\}^T \left[K_1^-\right] \{\mu^-\} + \{\psi^{F^-}\}^T \left[K_2^-\right] \{\mu^{F^-}\} \\ + \{\psi^{C^-}\}^T \left[K_3^-\right] \{\hat{\beta}^-\} = \{\psi^{W^-}\}^T \{V^-\} \end{aligned} \tag{3.26}$$

and

$$\{\hat{\gamma}^-\}^T \left[K_3^-\right]^T \{\mu^{C^-}\} + \{\hat{\gamma}^-\}^T \left[K_4^-\right]^T \{\hat{\beta}^-\} = 0 \tag{3.27}$$

All vectors $\{\psi^{F\pm}\}^T$, $\{\psi^{C\pm}\}^T$ and $\{\psi^{W\pm}\}^T$ are subsets of vector $\{\psi^{\pm}\}^T$, thus the preceding equations can be rearranged into a linear system with the stiffness matrices properly assembled. Since the vectors $\{\psi^{\pm}\}^T$ and $\{\hat{\gamma}^{\pm}\}^T$ are arbitrary, eq. (3.24) to (3.27) become a linear equation

$$[K]\{\mu\} = \{V\} \tag{3.28}$$

where

$$\{\mu\}^T = \left[\{\hat{\beta}^-\}^T, \{\mu^-\}^T, \{\mu^+\}^T, \{\hat{\beta}^+\}^T\right] \tag{3.29}$$

$$\{V\}^T = \left[\{V^-\}^T, \{V^+\}^T\right] \tag{3.30}$$

and the structure of the *global stiffness matrix* $[K]$ is given in Figure 3-2.

Gauss elimination is used to solve the matrix equation (3.28) for the vector $\{\mu\}$ which consists of the nodal point potentials in the finite element region and the expansion coefficients in the analytical region. Note that the global stiffness matrix $[K]$ is symmetric and real.

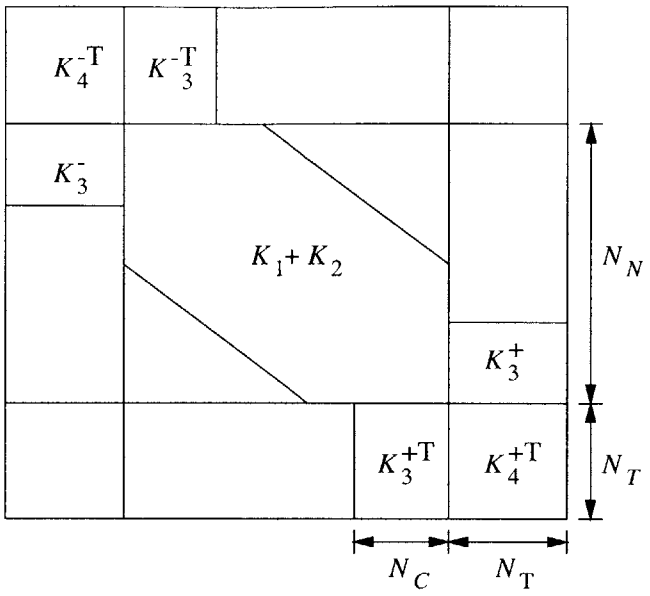

Figure 3-2: Global stiffness matrix $[K]$.

3.3 Stiffness matrix

In the finite element region, isoparametric 3-node elements are chosen. The Fourier-decomposed potential M in each element is approximated by

$$M = \{N^e\}^T \{\mu^e\} \tag{3.31}$$

where $\{\mu^e\}^T$ is a vector of nodal point values

$$\{\mu^e\}^T = (\mu_1^e, \mu_2^e, \mu_3^e)\,,$$

$\{N^e\}^T$ is the local shape function

$$\{N^e\}^T = (N_1^e, N_2^e, N_3^e)$$

and

$$N_i^e = (a_i + b_i x + c_i z)/2\triangle$$

$i = 1, 2, 3$, $\triangle$ is the area of the triangle element, and

$$\begin{cases} a_1 = x_2^e z_3^e - x_3^e z_2^e \\ b_1 = z_2^e - z_3^e \\ c_1 = x_3^e - x_2^e \end{cases} \quad \begin{cases} a_2 = x_3^e z_1^e - x_1^e z_3^e \\ b_2 = z_3^e - z_1^e \\ c_2 = x_1^e - x_3^e \end{cases} \quad \begin{cases} a_3 = x_1^e z_2^e - x_2^e z_1^e \\ b_3 = z_1^e - z_2^e \\ c_3 = x_2^e - x_1^e \end{cases}$$

For the lagoon side (the + region), the evaluation of the matrix $[K_1^+]$ in eq. (3.18) is calculated,

$$\begin{aligned} \left[K_1^+\right]_{3\times 3}^e &= \iint_A \nabla N_j^e \cdot \nabla N_i^e + \left(\frac{m\pi}{b}\right)^2 N_j^e N_i^e \, dA \\ &= \left[\frac{1}{4|\triangle|} K_{1ij}\right]^e \end{aligned} \tag{3.32}$$

where

$$K_{1ij} = b_i^2 + c_i^2 + \frac{2\triangle^2}{3}\left(\frac{m\pi}{b}\right)^2$$

when $i = j$, and

$$K_{1ij} = b_i b_j + c_i c_j + \frac{\triangle^2}{3}\left(\frac{m\pi}{b}\right)^2$$

when $i \neq j$. The element stiffness matrix is then assembled into a global matrix $[K_1^+]$. Note that $K_{1ij} = K_{1ji}$ thus $[K_1^+]$ is symmetric. In the assemblage, the nodal points are re-indexed and the element matrices are placed accordingly in the global matrix. The same node can belong to several adjacent elements and the stiffness contributions must be added up.

Similarly, we have

$$\left[K_2^+\right]_{2\times 2}^e = \left[-\frac{\omega^2}{g} K_{2ij}\right]^e \tag{3.33}$$

where

$$K_{2ij} = \frac{|x_2 - x_1|}{3}$$

when $i = j$, and

$$K_{2ij} = \frac{|x_2 - x_1|}{6}$$

when $i \neq j$, for points 1, 2 on the free surface.

The integration in eq. (3.21) is performed for points 1, 2 on the artificial boundary C^+:

$$\left[K_3^+\right]_{ij}^e = \left[\frac{\alpha_j e^{-\alpha_j C^+}}{k_j^2 |b_3|} K_{3ij}\right]^e \tag{3.34}$$

where there is no summation over j, with

$$K_{31j} = \cosh k_j(h + z_2) - \cosh k_j(h + z_1) + k_j b_3 \sinh k_j(h + z_1)$$

and

$$K_{32j} = \cosh k_j(h + z_1) - \cosh k_j(h + z_2) - k_j b_3 \sinh k_j(h + z_2)$$

Finally in eq. (3.23), the matrix $[K_4^+]$ is diagonal due to orthogonality, with the diagonal element

$$\left[K_4^+\right]_{ii} = -\alpha_i e^{-2\alpha_i C^+} \left[\frac{2}{h^+} + \frac{\sinh 2k_i h}{4k_i}\right] \tag{3.35}$$

The matrices for the $-$ region are similarly derived. Note that all matrix elements are real. These matrices are then properly arranged as in Figure 3-2 and constitute the global stiffness matrix $[K]$.

As in eq. (3.20), the matrix $[V^+]$ is evaluated by numerical integration of eq. (3.7) on the gate wall $x = \bar{\xi}^+$ for a given ω. Since the problem is two-dimensional, the vector product in eq. (3.7) is easily calculated by

$$|\bar{\mathbf{L}} \times \bar{\mathbf{n}}^+| = |\bar{\mathbf{L}}| \sin \kappa$$

where κ is the angle between $\bar{\mathbf{L}}$ and $\bar{\mathbf{n}}^+$. After $[K]$ and $[V]$ are derived, the vector $\{\mu\}$ is solved from the linear equation eq. (3.28). The results are then put in the eigen value equation eq. (2.50), which is satisfied after some iterations of ω. Similarly when computing C in eq. (2.52), we use

$$\bar{\mathbf{L}_c} \cdot \mathbf{e_3} = |\bar{\mathbf{L}_c}| \cos \kappa_G$$

where κ_G is the angle between $\bar{\mathbf{L}_c}$ and the positive z-axis.

The natural frequency ω and eigen function $M_m^{\pm}$ are then found. Some one-

dimensional root-finding routines can be used here. Since the calculation of $I_a(\omega)$ is somewhat computationally expensive, and the eigen value equation is well-behaved, we choose the *secant method*, which generally converges rapidly, to find ω in eq. (2.50).

For a particular choice in the finite element region, we must choose small enough elements in a wavelength, and a large enough number of expansion terms N_T. The accuracy is first judged by comparison with the analytical solution and then by convergence tests with different choices of element size and N_T.

Chapter 4

Numerical results

As a check we first performed calculations for Mode One of the simplified model of vertically standing gates with rectangular cross section, as studied analytically and experimentally by Mei *et al.* [9]. The water depths are kept the same on both sides of the gates. We have also performed a wide range of computations for inclined gates of rectangular cross section and a flat seabed. Even when the gross dimensions are the same as those in the proposed design, the results do not compare well with the experiments by Delft Hydraulics Laboratory [12]. Some theoretical derivations are given in Appendix A with a simple numerical result, which is not satisfactory. This is because the total moment C and the hydrodynamics inertia I_a depend strongly on the geometry of the gate and the housing: the more accurate model is necessary. Therefore, the prototype geometry as shown in Figure 2-2 is used. By varying the parameters including water depth difference, inclination angle, gate width, and thickness, the role of the gate geometry on the eigen-period is examined and compared with existing laboratory experiments [12].

4.1 Vertical gates

A simplified model where the gates are rectangular and vertical is solved numerically here. The analytical solution is adapted from Mei *et al.* [9] and Sammarco [13], where

the total moment C and the hydrodynamics inertia I_a are derived explicitly:

$$C = \rho g a h^2 - Mg(z_c + h) \tag{4.1}$$

with $2a$ being the thickness of the gate and z_c the depth of the center of mass. Also

$$I_a(\omega) = \frac{2\rho b}{\pi} \sum_{m=1}^{\infty} \sum_{n=0}^{\infty} \frac{1}{m} \beta_{mn} D_n \sin m\pi(1-r) \tag{4.2}$$

with

$$\beta_{mn} = \frac{b_m Dn}{\alpha_{mn} C_n} \tag{4.3}$$

where

$$C_0 = \frac{1}{2}\left(h + \frac{g}{\omega^2}\sinh^2 kh\right), \quad D_0 = \frac{1}{k^2}\left[\left(\frac{h\omega^2}{g} - 1\right)\cosh kh + 1\right], \tag{4.4}$$

$$C_n = \frac{1}{2}\left(h - \frac{g}{\omega^2}\sin^2 k_n h\right), \quad D_n = \frac{1}{k_n^2}\left[\left(1 - \frac{h\omega^2}{g}\right)\cos k_n h - 1\right]. \tag{4.5}$$

b_m and α_{mn} are given in eq. (2.45) and eq. (3.2) accordingly. For Mode One, analytical and numerical results are compared in Figure 4-1. Different gate inertias are examined, from the lowest to the highest, $I = 0.21$, 0.196, 0.273, 0.582 and 0.771 $\mathrm{kg\,m^2}$, as being tested by Tran [17].

A sample free surface displacement is shown for $I = 0.21\mathrm{kg\,m^2}$ in Figure 4-2, where

$$\zeta = \eta e^{-i\omega t} + * \tag{4.6}$$

with

$$\eta = \frac{i}{\omega} \sum_{m=1}^{\infty} \frac{\partial M_m}{\partial z} \cos\left(\frac{m\pi y}{b}\right) \tag{4.7}$$

The width of the wave flume in the experiment is 0.366 m which equals the semi-period b in the y direction. Note that the free surface displacement is opposite to the gate motion, that is, the gate oscillation is *forced* by the waves, instead of generating them. This is reasonable since waves are *trapped* near the gates, there is no radiation towards infinity.

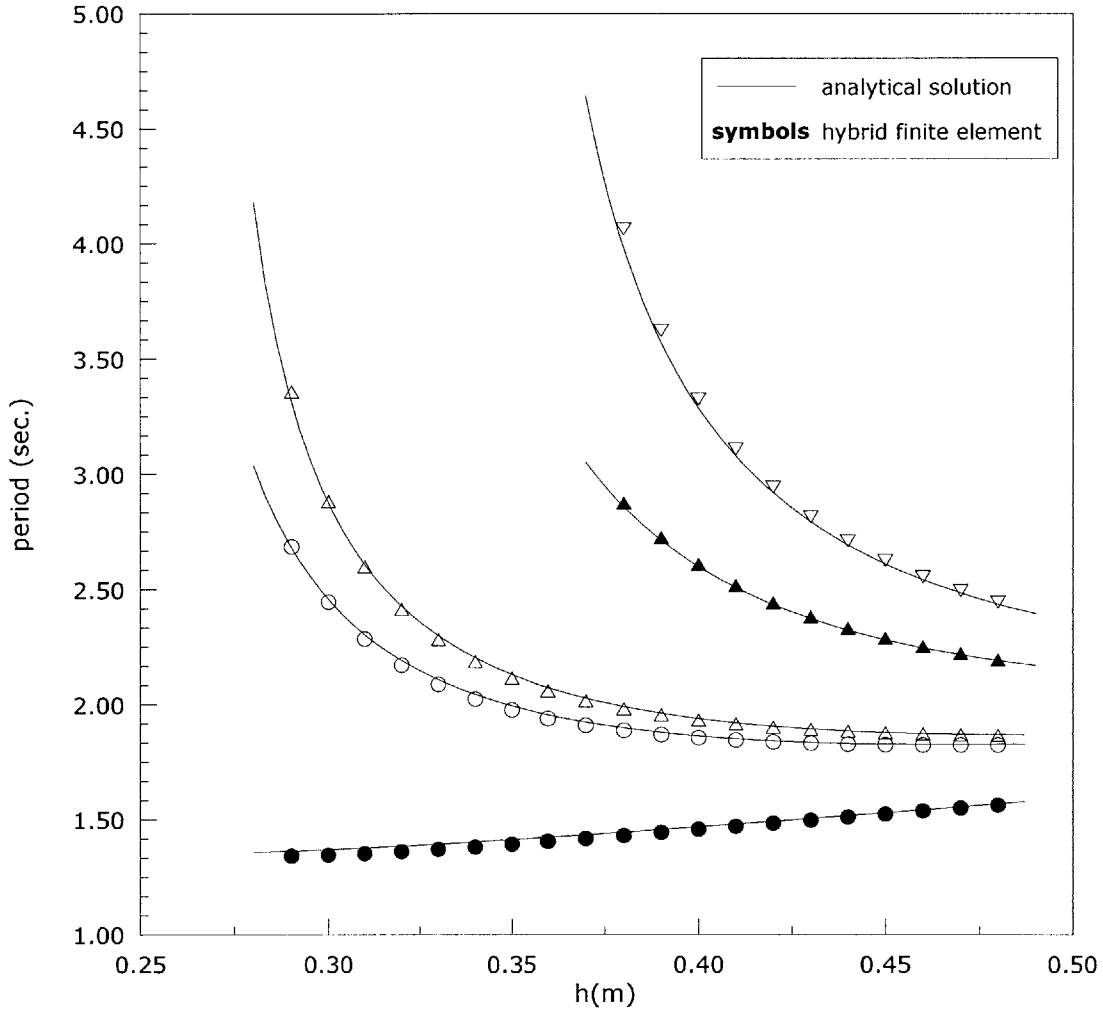

Figure 4-1: Natural period of vertical gates oscillating in opposite phases in various water depths h (m). Corresponding to curves from the lowest to the highest, the inertia I is 0.21, 0.196, 0.273, 0.582, 0.771 kg m^2.

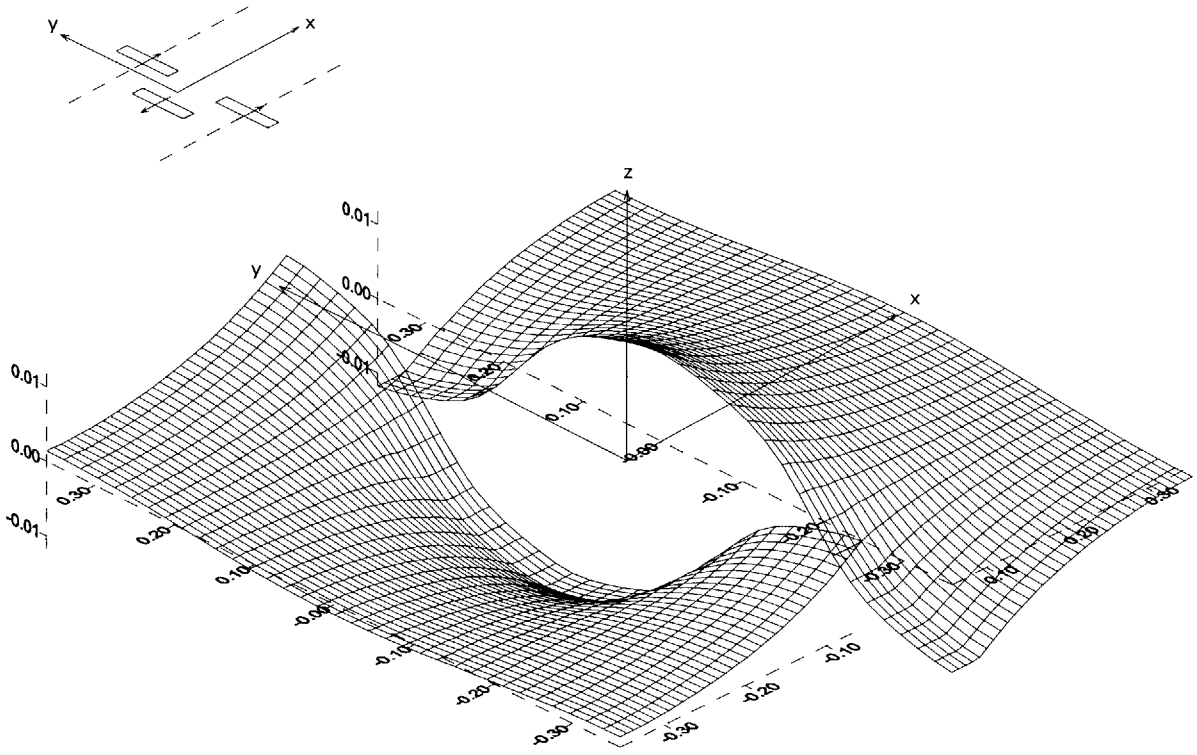

Figure 4-2: Free surface displacement for vertical gates at Mode One. $I = 0.21\text{kg}\,\text{m}^2$, $\omega = 4.0$ and $h = 0.4$ m.

4.2 Prototype gates

4.2.1 Scale model experiments

The dimensions of the proposed design to span the Malamocco inlet are shown in Figure 4-3, with width $b = 20$ m in y direction, and thickness of 4 m. In calm weather, the water depth is 15 m on both sides of the gate. In a severe storm, the water level is expected to increase by 0.5 m in the lagoon and up to 2.5 m on the sea side, implying a difference of water levels ranging from 0 to 2 m. When in operation, the gates are raised to an inclination angle of $\bar{\Theta}$=50° from the horizon.

Under contract with Consorzio Venezia Nuova, Delft Hydraulics Laboratory [12] performed a series of scale model experiments during 1988 to study the oscillations of the gates. The model gates consisted of polyurethane foam and covered with aluminum sheeting; the air chamber was not reproduced. Instead of water, lead ballast, put inside an aluminum cylinder installed in the center plane of the model gate along the z-axis, was used to balance the inclination and water-depth difference. The total mass, position of center of gravity, and structural moment of inertia were thus not reproduced. We shall now describe our mathematical simulations for these model gates with a dual purpose of predicting and understanding the effects of various geometrical parameters, and of comparing our theory with the Delft measurements. It should be noted that while the inertia properties (total mass, position of center of gravity, and structural moment of inertia) of the model gates are different from the proposed prototype, the numerical results given in the followings are, however, transformed to prototype scale as done in the Delft report [12].

For our mathematical model we need to know the position vector $\bar{\mathbf{L}}_\mathbf{c}$ of the center of gravity of the gate, as well as the structural inertia I. For the laboratory model, both can be found by linear interpolation from the recorded percentage of ballast lead (Fig 5.1, Fig 5.2, Fig 5.4 and table on p 37 in the Delft report [12]) and are listed in Table 4.1 and 4.2. All these values have been converted by Delft Hydraulic Laboratory from model scale to prototype scale.

In general, higher percentage of ballast lead gives larger $Mg\bar{\mathbf{L}}_\mathbf{c}$ and I. Some of the

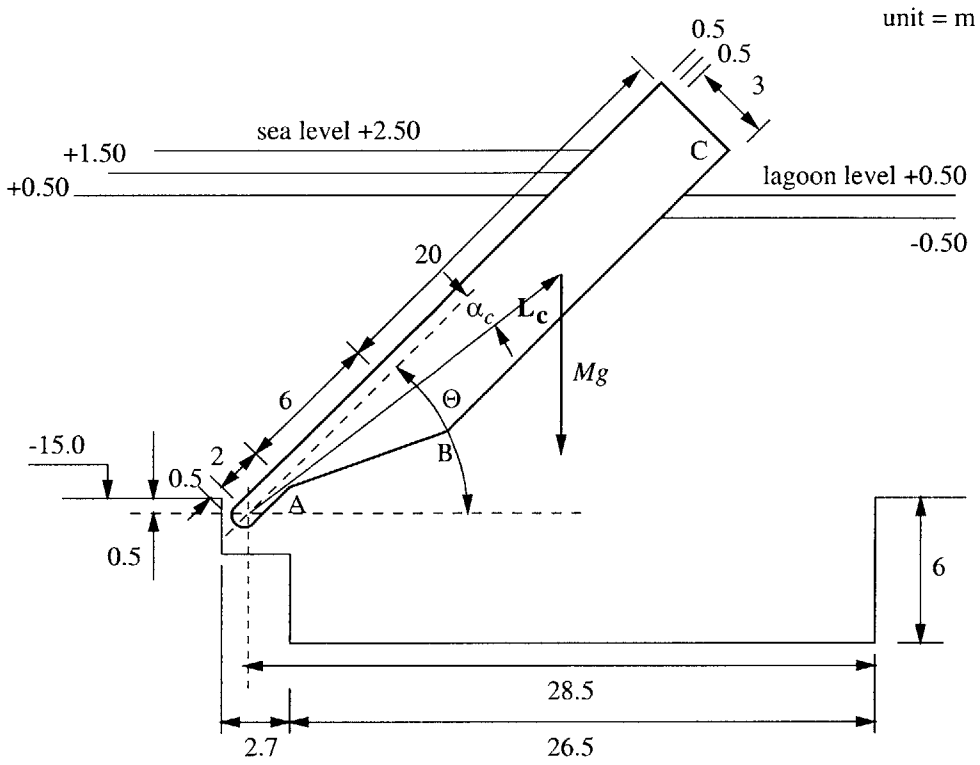

Figure 4-3: Prototype geometry. The dimensions shown in meters are for the Malamocco inlet, with width $b = 20$ m in y direction, thickness = 4 m, and inclination angle $\bar{\Theta} = 50°$ when in operation.

	$h^- - h^+$ (m)					
inertia properties	−0.5	0.0	0.5	1.0	1.5	2.0
percent lead (%)	86.97	74.17	61.36	48.55	29.68	10.81
I (10^6kg m^2 per m gate width)	21.91	17.39	13.73	11.27	8.06	6.56
$\lvert\bar{\mathbf{L}}_\mathbf{c}\rvert$ (m)	16.23	15.31	14.52	13.94	13.38	14.04
angle α_c (see Figure 4-3)	4.96	5.20	5.44	5.64	5.84	5.56

Table 4.1: Values of $\bar{\mathbf{L}}_\mathbf{c}$ and I. For $\bar{\Theta}$=50°, h^+=15.5 m.

inertia properties	$\bar{\Theta}$					
	40°	45°	50°	55°	60°	65°
percent lead (%)	102.1	88.13	74.17	64.64	55.11	45.58
I (10^6kg m^2 per m gate width)	27.24	22.32	17.39	14.36	12.53	10.70
$\lvert\bar{\mathbf{L}}_\mathbf{c}\rvert$ (m)	17.24	16.31	15.31	14.67	14.23	13.83
angle α_c (see Figure 4-3)	4.73	4.94	5.20	5.40	5.54	5.68

Table 4.2: Values of $\bar{\mathbf{L}}_\mathbf{c}$ and I. For $h^{\pm}$=15.5 m.

scale model tests were for free-oscillations where the gates were given initial angular displacements consistent with the mode. Because only three or four gates were used to span the width of the wave channel, records of natural periods are available only for Mode One and Two as shown in Figure 2-1. Specifically, natural periods have been recorded for Gate N°7 for several values of (i) inclination angles and (ii) water-level differences across the barrier. Our numerical results can only be compared with these measurements.

4.2.2 Hydrodynamic inertia and total moment

To help understand the results on the natural periods, we first present the calculated hydrodynamic inertia I_a as a function of ω. Since the total moment C and structural inertia I depend only on the equilibrium geometry, they are independent of ω, *i.e.*, are constants for fixed $\bar{\Theta}$ and $h^{\pm}$. As shown in Figure 4-4, the hydrodynamic inertia I_a for $\bar{\Theta} = 50°$ is around 10^8kg m^2, and for the scale model, the structural inertia I, which is a constant here, is of the same order $O(10^8)$. Therefore both I_a and I are important in the calculation of the eigen solution ω in eq. (2.50). Because I is a constant, and $I_a(\omega)$ increases monotonically with ω, eq. (2.50) has only one root. Also the eigen frequency is lower (period is longer) if the hydrodynamic inertia is greater.

Since the eigen frequency is determined by the hydrodynamic inertia I_a as well as I, let us study first their dependence on various geometrical dimensions. First, the effect of water level difference is examined. The water depth in the lagoon h^+ is

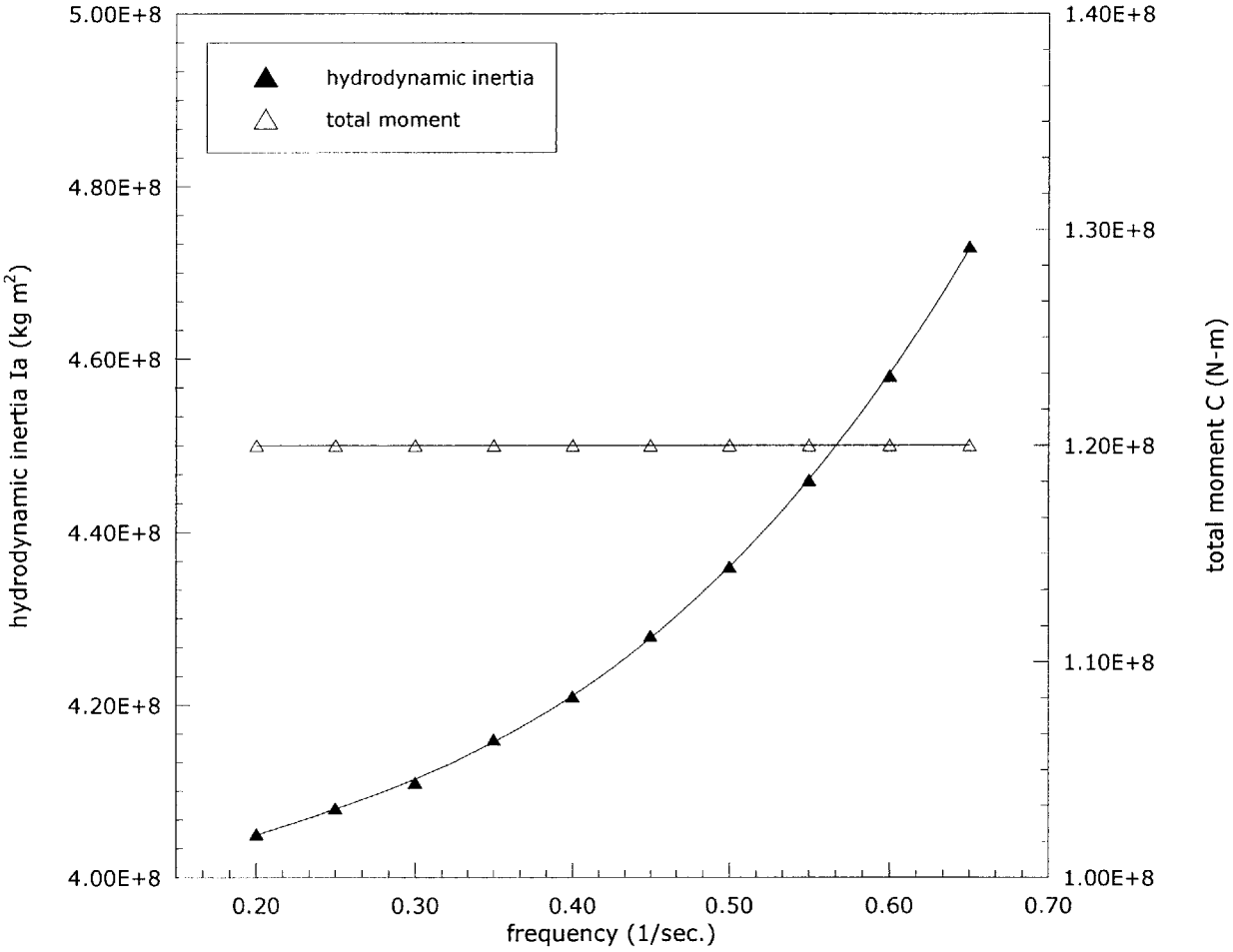

Figure 4-4: Calculated hydrodynamic inertia $I_a(\omega)$ and total moment C of a half gate for various frequencies. Mode One, $\bar{\Theta} = 50°$, $h^{\pm}$=15.5 m, b=20 m.

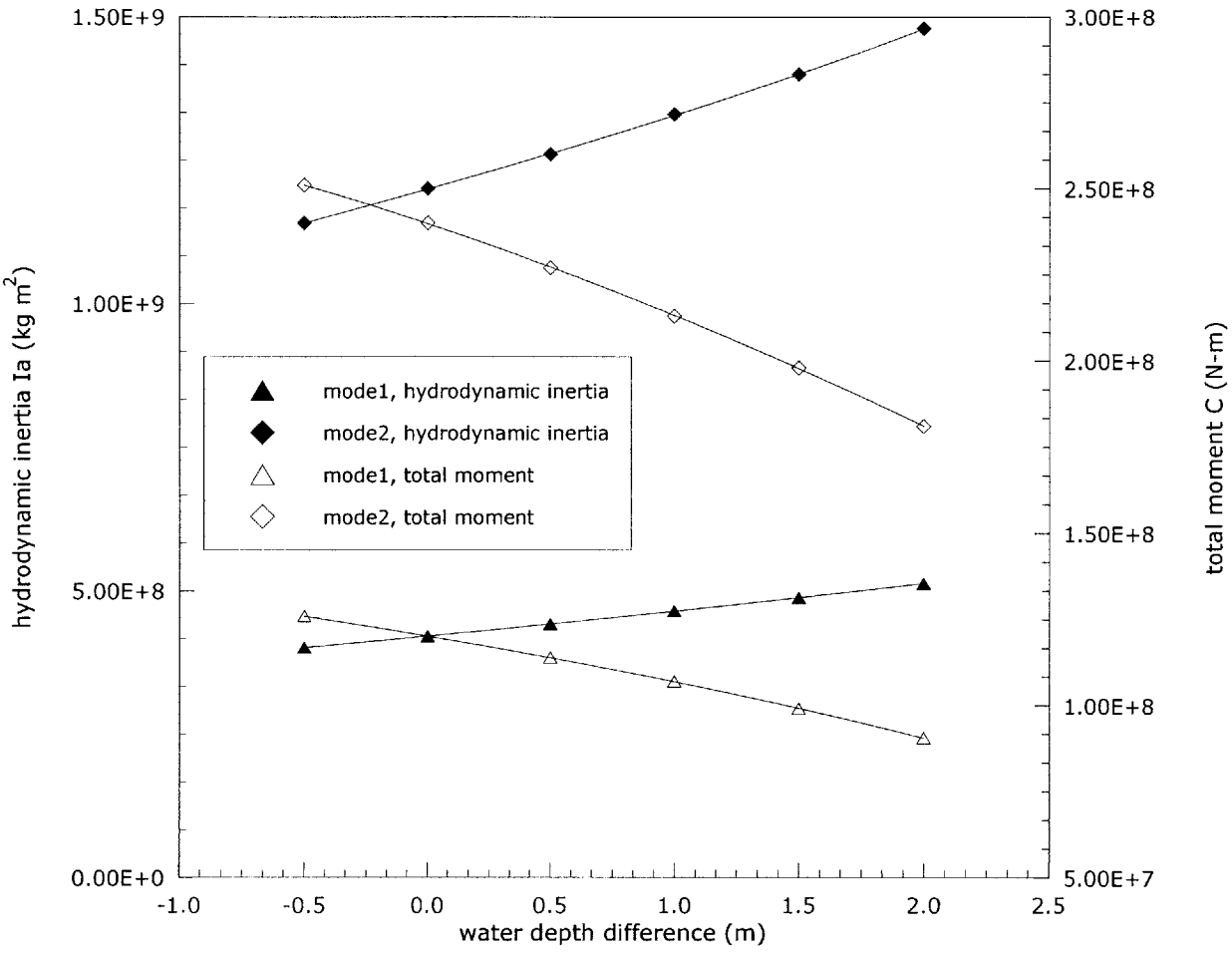

Figure 4-5: Calculated hydrodynamic inertia I_a and total moment C with various water depth differences. Prototype geometry is used with ω=0.4, $\bar{\Theta} = 50°$, b=20 m, h^+=15.5 m, $h^- = h^+$+water depth difference. (Mode One: half gate; Mode Two: one gate.)

	$h^- - h^+$ (m)					
$C/(I_a + I)$	−0.5	0.0	0.5	1.0	1.5	2.0
Mode One	0.2032	0.2017	0.1968	0.1852	0.1743	0.1564
Mode Two	0.1590	0.1551	0.1479	0.1369	0.1268	0.1123

Table 4.3: The ratio $C/(I_a + I)$ for various water depth differences. ω=0.4, $\bar{\Theta}$=50°, b=20 m.

kept constant at 15.5 m, while h^- on the sea side is varied from 15.0 to 17.5 m. The frequency ω=0.4 here is arbitrarily fixed. When h^- increases, $Mg\bar{\mathbf{L}}_\mathbf{c}$ must decrease in eq. (2.39), then the total moment C decreases as well in eq. (2.52), as shown in Figure 4-5. In the scale model, a decrease in $Mg\bar{\mathbf{L}}_\mathbf{c}$ also implies a decrease in I. With increasing water level difference, C and I decrease but I_a increases, hence in eq. (2.50), the change of $(I_a + I)$ is small. In Table 4.3, it can be found that an increased difference in water levels reduces the ratio $C/(I_a + I)$, therefore lengthens the period. However, within the design range, the ratio does not vary significantly, so the water level difference across the barrier is not a major factor influencing the eigen frequency ω.

In Figure 4-6, the water depths $h^\pm$ are kept constant on both sides at 15.5 m, the frequency ω is fixed, but the inclination angle $\bar{\Theta}$ ranges from 40° to 65°. It is shown that I_a and C change rapidly with the inclination angle, and both decrease with increasing $\bar{\Theta}$. In the extreme case when the gate becomes vertical, I_a and C approach their minima. Also in the model tests, I decreases as $\bar{\Theta}$ increases. As shown in Table 4.4, the ratio of $C/(I_a + I)$ decreases monotonically with increasing inclination angle, so a longer period is expected for larger $\bar{\Theta}$. In comparison with Table 4.3, trapped wave periods are much more sensitive to the inclination angle than the difference in water levels.

Finally in Figure 4-7, we show the effect of the gate width b in the y direction (along the barrier) for fixed $\bar{\Theta}$ and $h^\pm$. Because C and I are not dynamical quantities, they are proportional to the gate width. I_a, however, increases more dramatically when b increases, thus $C/(I_a + I)$ must decrease with wider gates, leading to longer trapped

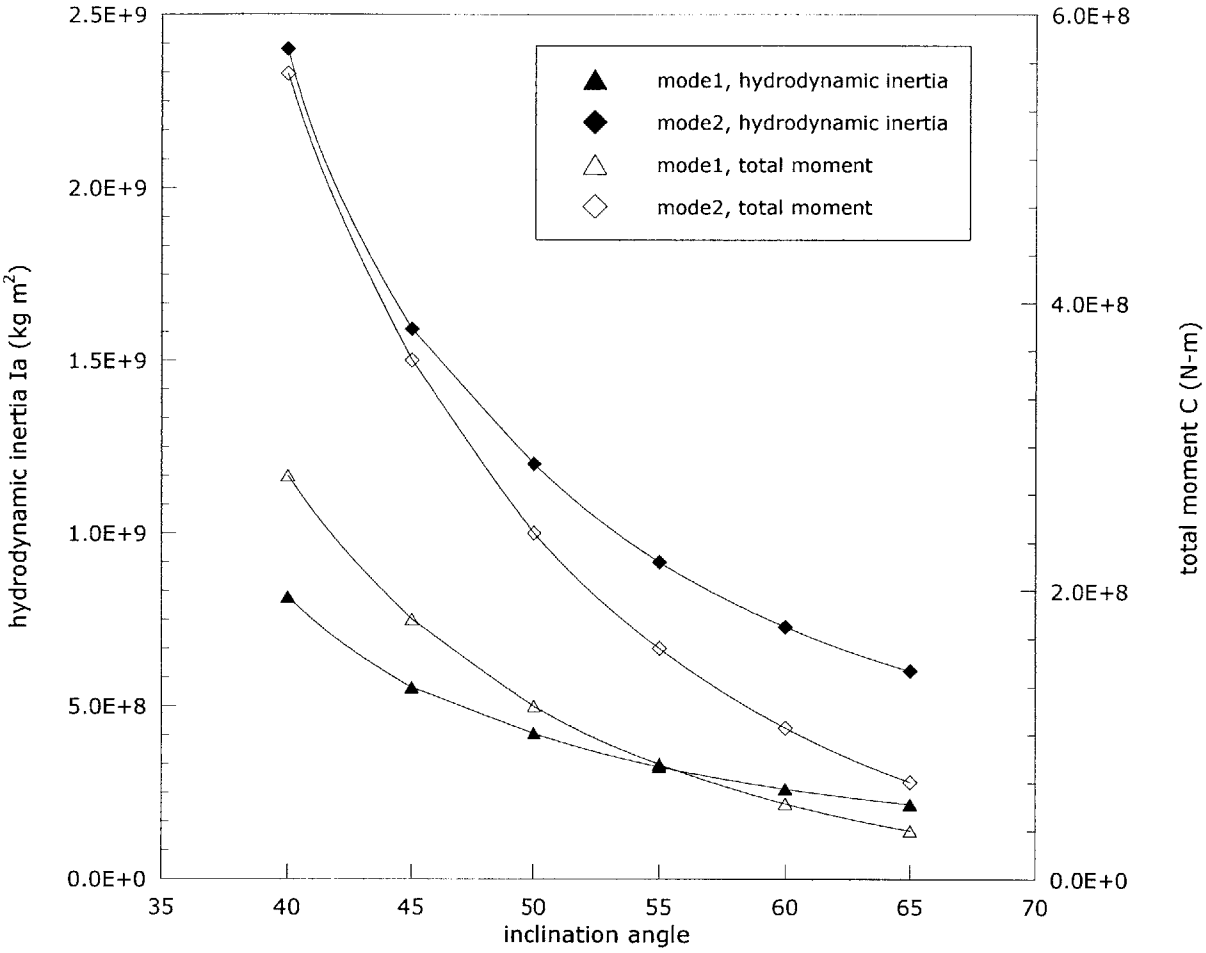

Figure 4-6: Calculated hydrodynamic inertia I_a and total moment C with various inclination angles for prototype geometry. ω=0.4, $h^{\pm}$=15.5 m, b=20 m. (Mode One: half gate; Mode Two: one gate.)

	$\bar{\Theta}$					
$C/(I_a + I)$	40°	45°	50°	55°	60°	65°
Mode One	0.2708	0.2476	0.2149	0.1823	0.1537	0.1193
Mode Two	0.1970	0.1858	0.1628	0.1402	0.1180	0.0921

Table 4.4: The ratio $C/(I_a + I)$ for various inclination angles. ω=0.4, $h^{\pm}$=15.5 m, b=20 m.

wave period from eq. (2.50).

4.2.3 Natural periods of trapped waves

With the effects of I_a and C understood, we can now examine quantitatively the natural periods of trapped waves and compared them with measured data.

First we keep $\bar{\Theta} = 50°$ and h^+=15.5 m as in Figure 4-5, and vary h^- on the sea side. In Figure 4-8, the trapped wave period increases with the water level difference for both Modes One and Two, as predicted from Figure 4-5. For the same gate geometry, an increase in depth difference lengthens the period. However, water level difference across the barrier is not a major factor. The agreement between numerical result and experiment data is fair.

In Figure 4-9, the effect of static angle of inclination $\bar{\Theta}$ is examined. Only for Mode Two is comparison possible because the experiment was performed for three gates across the width of the flume. The agreement is good. When the equilibrium inclination approaches 90°, the trapped mode period increases. This suggests that without changing the gate dimensions, vertical gates may be more advantageous in having natural frequencies far below the incident wave spectrum.

In Figure 4-10, the gate width in the y direction is varied. In the Delft experiments only one width $b = 20.0$ m was examined. The agreement is again good. As shown in the figure, if two adjacent gates are locked together, *i.e.*, $b = 40.0$ m, the period increases by about 30%. Therefore locking two or more gates can also help reducing the likelihood of resonance by making the eigen period longer than the period of the significant incident waves.

Numerical experiments on the effects of gate thickness are shown in Figure 4-11. Both water depth $h^{\pm}$ and inclination angle $\bar{\Theta}$ are kept constant. Referring to Figure 4-3, in the computations we increase the gate thickness by moving the wall BC away from the opposite wall, while keeping the slope of segment AB the same. Various values of the gate thickness are then tested. Since the structural moment of inertia I and the position of center of gravity $\bar{\mathbf{L}}_\mathbf{c}$ are not available from the Delft report, we simply take I and inclination of $\bar{\mathbf{L}}_\mathbf{c}$ as constants. Physically we can expect a smaller

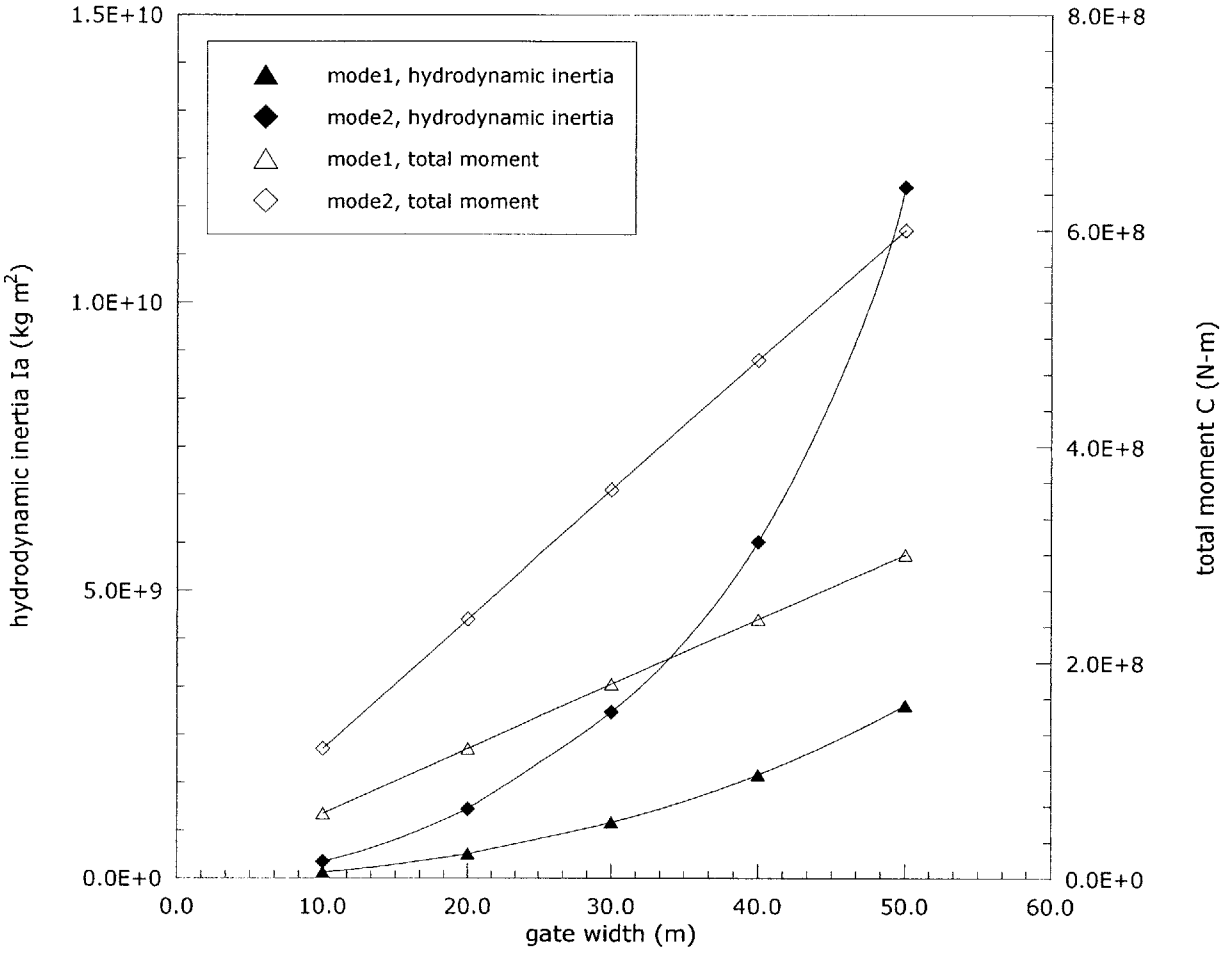

Figure 4-7: Calculated hydrodynamic inertia I_a and total moment C for various gate widths b. ω=0.4, $\bar{\Theta} = 50°$, $h^{\pm}$=15.5 m. (Mode One: half gate; Mode Two: one gate.)

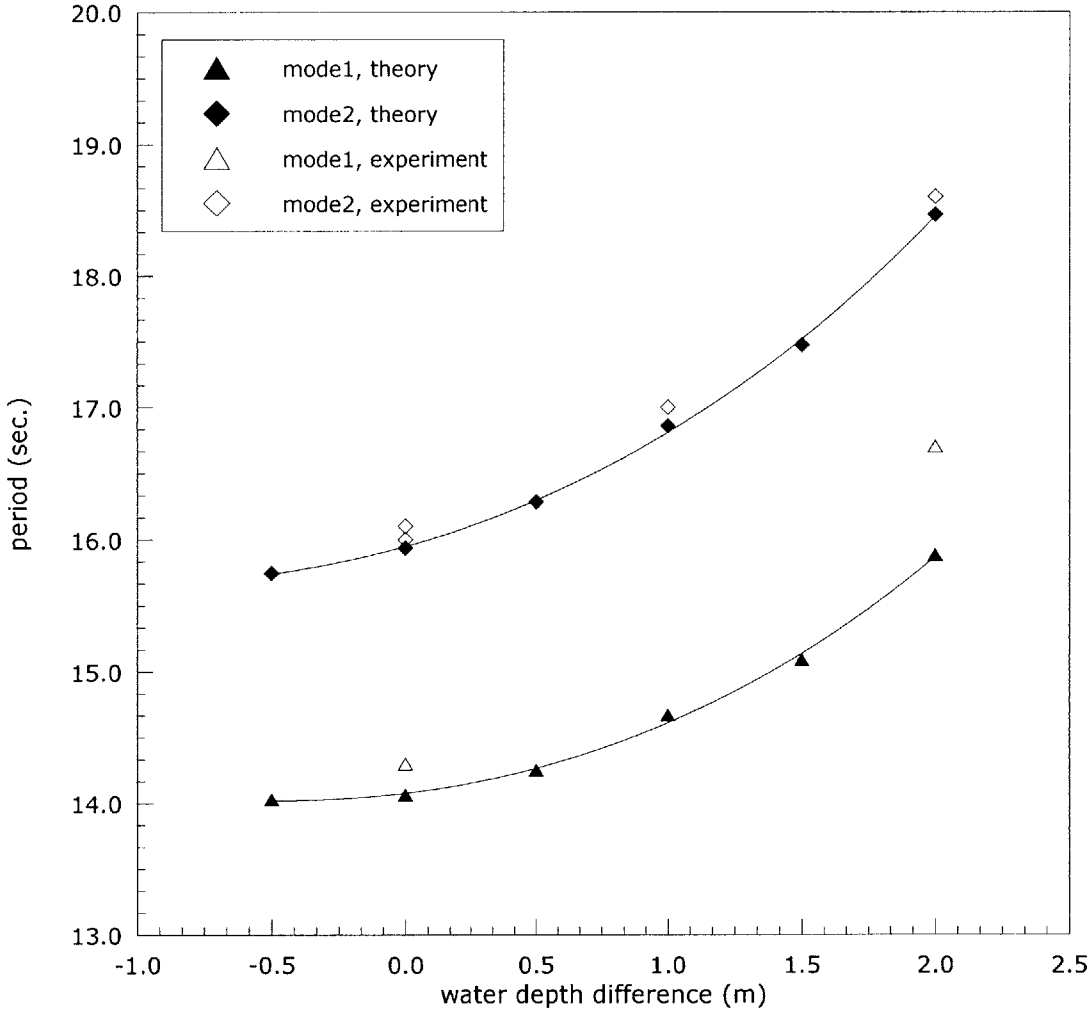

Figure 4-8: Natural period of trapped mode for various water depth differences. $\bar{\Theta} = 50°$, b=20 m, h^+=15.5 m, $h^- = h^+$+water depth difference.

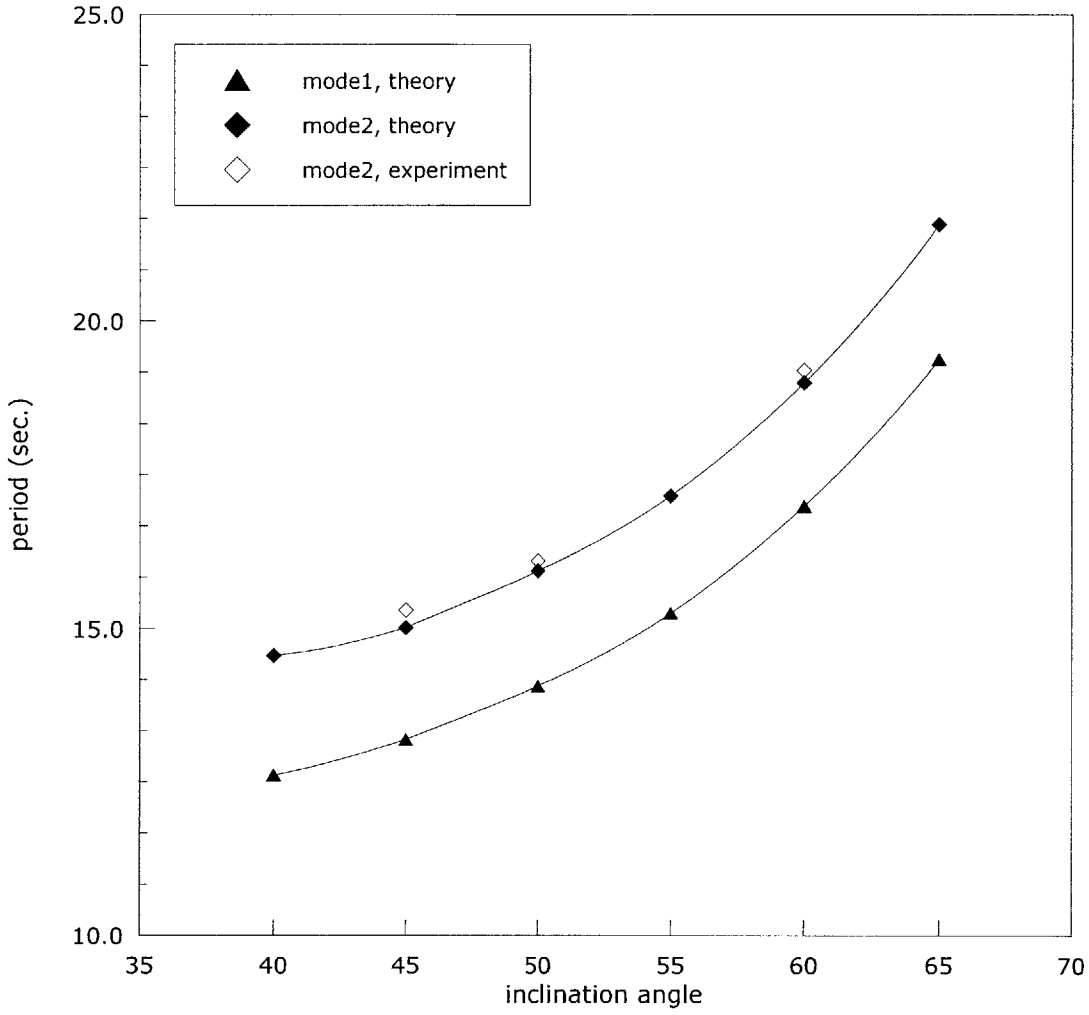

Figure 4-9: Natural period of trapped mode for various inclination angles. $h^{\pm}$=15.5 m, b=20 m.

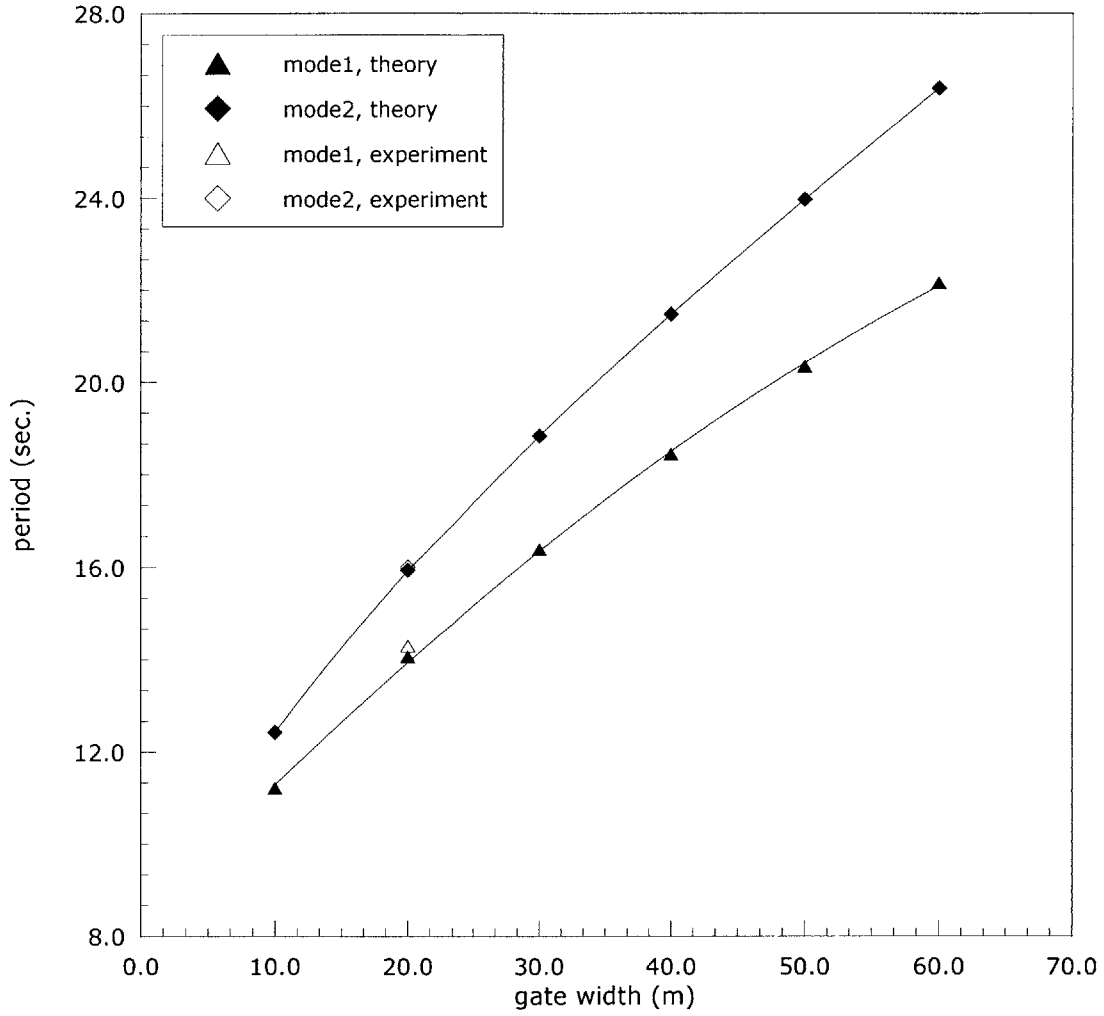

Figure 4-10: Natural period of trapped mode for various gate widths. $\bar{\Theta} = 50°$, h^+=15.5 m.

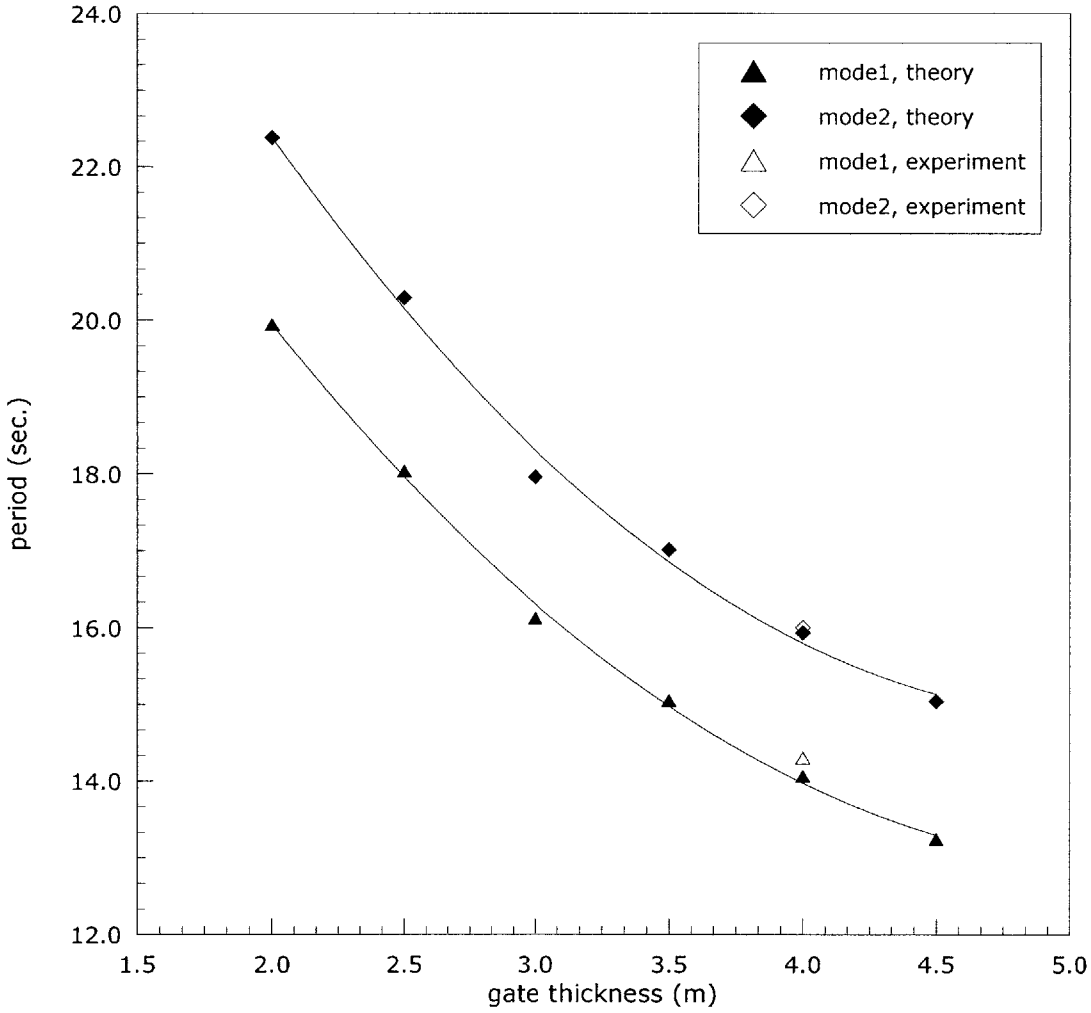

Figure 4-11: Natural period of trapped mode for various gate thicknesses. $\bar{\Theta} = 50°$, $h^{\pm}$=15.5 m, b=20 m.

I and a larger inclination of $\bar{\mathbf{L}}_{\mathbf{c}}$ for a thinner gate. Agreement with the limited data is good. For thicker gates, the opening due to out-of-phase oscillations will of course be smaller for the same angular displacement, but the reduction of natural period may make the barrier more susceptible to resonance by incident waves whose spectral peak is around 14 s in Adriatic Sea.

As was pointed out in Mei *et al.* [9], higher modes are characterized by longer spatial periods b relative to the width of each gate, *i.e.*, there are more gates in a period $2b$ along the barrier. From our computations it can be seen that the natural period of Mode One is shorter than that of Mode Two which has three gates in a spatial period. Therefore if the gates are designed such that the peak period of the incident waves is much smaller than the natural period of Mode One, subharmonic resonance of Mode Two, or even higher modes, poses no threat.

As can be seen from Figures 4-8 through 4-11, agreement between our numerical predictions and the Delft experiments is quite good in general. The largest error is about 5% in Figure 4-8, for Mode One, when the water depth difference is 2 m.

Chapter 5

Conclusion

Extending the linear theory of Mei *et al.* [9], the problem of trapped modes near inclined Venice storm gates is examined by using the hybrid finite element method. Natural periods of the trapped waves are computed to assess the influence of geometrical parameters, and compared with experiments, for the prototype geometry. This numerical scheme makes it possible to consider a wide range of gate inclination, thickness, width, etc., which are factors in exciting resonance and in cost estimates. Variable bathymetry and water level difference across the barrier are also considered. For a fixed geometry of the gate, we have shown that the increase of water level difference, or an increase of gate inclination angle, is accompanied by a longer natural period. The trapped wave period also becomes longer when the gate width is extended. Finally, the effect of thicker gate is to decrease the eigen-period.

To avoid unwanted resonance, we can adjust the gate dimensions so that the natural frequency of the gates is outside the range of the local incident wave spectrum. Since in Mode One there is an opening between every pair of adjacent gates, it is the worst mode for the intended function of the barrier. Either by reducing the gate thickness, by increasing the gate width, or by maintaining a more vertical equilibrium position, the eigen-period can be increased so as to escape the effective range of the incident wave frequencies. Indeed the simplest solution appears to be just locking two, or more, or all gates together.

For unlocked gates, further development of the theory along the lines of Sam-

marco *et al.* [14][15] would lead to a nonlinear evolution equation for the trapped wave, and the study of spectral shape of the incident waves is also necessary.

Appendix A

A simplified model

A.1 Formulation

Referring to Figure A-1, consider the simplified gate model of rectangular cross section with the thickness of $2a$, as used in Mei *et al.* [9]. Assume a flat seabed of constant depth: $z = h^+$ on the lagoon side while $z = h^-$ on the sea side. The walls of the gate are then given:

$$\begin{aligned} \xi^+ &= (z + h^+)\cot\Theta + \left(\frac{a}{\sin\Theta}\right) \\ \xi^- &= (z + h^-)\cot\Theta - \left(\frac{a}{\sin\Theta}\right) \end{aligned} \tag{A.1}$$

therefore the boundary condition on the gate walls becomes

$$\frac{\partial\phi^\pm}{\partial x}\tan\Theta = \frac{\partial\phi^\pm}{\partial z} + \frac{(z + h^\pm) \pm a\cos\Theta}{\sin\Theta\cos\Theta}\left(\frac{d\Theta}{dt}\right) \tag{A.2}$$

at $x = \xi^\pm$, and eq. (2.17) reads

$$\begin{aligned} -I\frac{d^2\Theta}{dt^2} = Mg\,d_c\cos\Theta \;+\; & \int_\Lambda\int_{z=-h^-}^{Z^-} \frac{P}{\sin\Theta}\left(\frac{z + h^-}{\sin\Theta} - a\cot\Theta\right) dy\,dz \\ -\; & \int_\Lambda\int_{z=-h^+}^{Z^+} \frac{P}{\sin\Theta}\left(\frac{z + h^+}{\sin\Theta} + a\cot\Theta\right) dy\,dz \end{aligned} \tag{A.3}$$

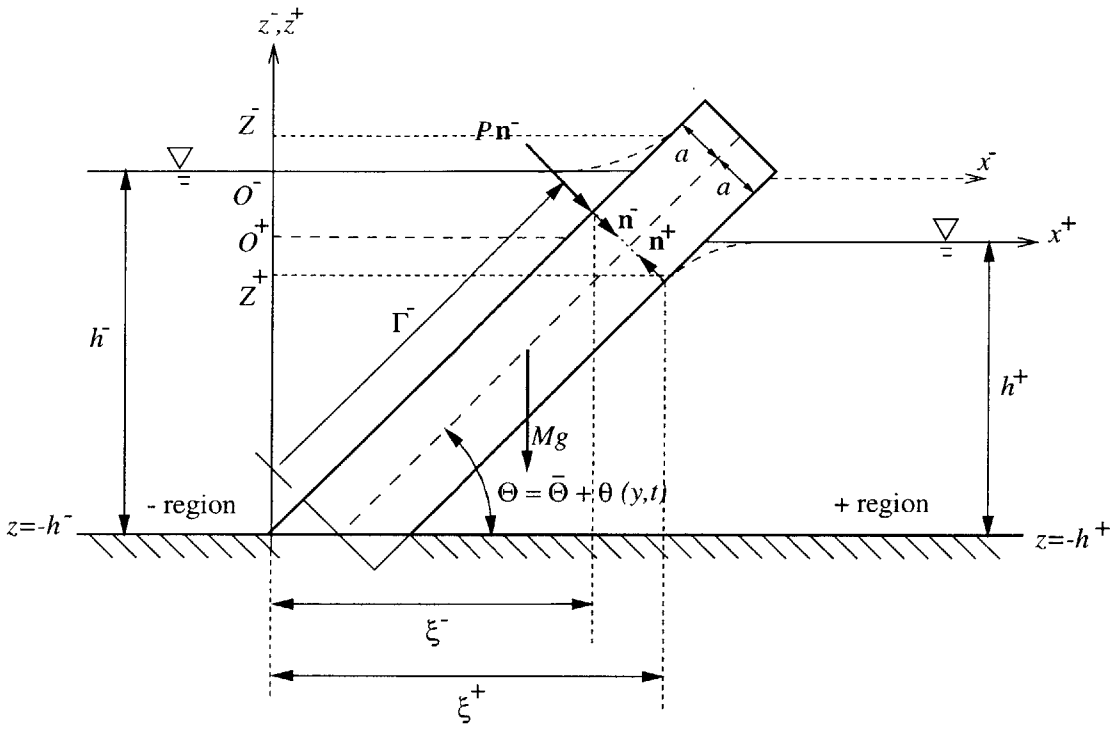

Figure A-1: The ideal gate model.

in $-y$ direction, with d_c being the distance of the center of gravity of the gate from the hinge. Notice that as in eq. (2.17), we have, for change of variable,

$$\frac{ds}{dz} = \frac{1}{\sin\Theta}$$

The preceding equations are similarly normalized as in Section 2.2, where

$$\mathbf{x}' = \mathbf{x}/b,\ t' = \omega t,\ \phi' = \frac{\phi}{A\omega b},\ \zeta' = \zeta/A,\ h'^{\pm} = h^{\pm}/b$$

and

$$\theta' = \frac{\Theta - \bar{\Theta}}{\epsilon} = \frac{\theta}{\epsilon}$$

Taylor expansion is then performed to linearize all the boundary conditions.

For the free surface boundary condition, eq. (2.21) is given at $z' = \epsilon\zeta'$. After

Taylor expansion about $z' = 0$, we have

$$G\left(\frac{\partial\phi'}{\partial z'} + \frac{\partial^2\phi'}{\partial z'^2}\cdot\epsilon\zeta' + \cdots\right)_{z'=0} + \left(\frac{\partial^2\phi'}{\partial t'^2} + \frac{\partial^3\phi'}{\partial t'^2\partial z'}\cdot\epsilon\zeta' + \cdots\right)_{z'=0} + \epsilon\frac{\partial}{\partial t'}|\nabla'\phi'|^2 + \frac{1}{2}\epsilon^2\nabla'\phi'\cdot\nabla'|\nabla'\phi'|^2 + \cdots = 0 \tag{A.4}$$

As $\epsilon \to 0$, it gives exactly eq. (2.26). Similarly, at the walls of the gate $\xi'^{\pm}$

$$x' = (z' + h'^{\pm})\cot(\bar{\Theta} + \epsilon\theta') \pm \frac{a'}{\sin(\bar{\Theta} + \epsilon\theta')} \tag{A.5}$$

Apply Taylor expansion

$$\begin{cases} \tan(\bar{\Theta} + \epsilon\theta') = \tan\bar{\Theta} + \epsilon\theta'\cdot\sec^2\bar{\Theta} + \frac{1}{2}\epsilon^2\theta'^2\cdot\sec^2\bar{\Theta}\cot\bar{\Theta} + O(\epsilon^3) \\ \cos(\bar{\Theta} + \epsilon\theta') = \cos\bar{\Theta} - \epsilon\theta'\cdot\sin\bar{\Theta} - \frac{1}{2}\epsilon^2\theta'^2\cdot\cos\bar{\Theta} + O(\epsilon^3) \\ \sin(\bar{\Theta} + \epsilon\theta') = \sin\bar{\Theta} + \epsilon\theta'\cdot\cos\bar{\Theta} - \frac{1}{2}\epsilon^2\theta'^2\cdot\sin\bar{\Theta} + O(\epsilon^3) \end{cases} \tag{A.6}$$

we find the mean position of the walls $x' = \bar{\xi}'^{\pm}$ to be

$$x' = (z' + h'^{\pm})\cot\bar{\Theta} \pm \frac{a'}{\sin\bar{\Theta}} \tag{A.7}$$

The boundary condition at the walls of the gate can therefore be expanded about $x' = \bar{\xi}'^{\pm}$. By letting $\epsilon \to 0$, we find

$$\frac{\partial\phi'^{\pm}}{\partial\bar{n}^{\pm}} = \frac{\mp(z' + h'^{\pm}) - a'\cos\bar{\Theta}}{\sin\bar{\Theta}}\frac{d\theta'}{dt'} \tag{A.8}$$

at $x' = \bar{\xi}'^{\pm}$. The unit normal vector $\bar{\mathbf{n}}^{\pm} = \mp(\sin\bar{\Theta}, -\cos\bar{\Theta})$ points into the gate at the mean position.

After substituting eq. (A.6) into the normalized equation of eq. (A.3), and keeping the terms up to $O(\epsilon)$, the dynamic condition of the gate can be rewritten

$$-\epsilon\frac{I}{\rho b^5}\frac{d^2\theta'}{dt'^2} = \frac{M}{\rho b^3}G\,d'_c\cos\bar{\Theta} - \epsilon\frac{M}{\rho b^3}G\,d'_c\sin\bar{\Theta}\theta' + \int_{\Lambda'}dy'\times \left\{-\int_{-h'^-}^{\epsilon\zeta'^-}\frac{Gz'\Gamma'^-}{\sin\bar{\Theta}}dz' - \epsilon\int_{-h'^-}^{\epsilon\zeta'^-}\frac{1}{\sin\bar{\Theta}}\left[Gz'\theta'\left(2\cot\bar{\Theta}\Gamma'^- - a'\right) + \frac{\partial\phi'^-}{\partial t'}\Gamma'^-\right]dz'\right. \tag{A.9}$$

$$+\int_{-h'^{+}}^{\epsilon\zeta'^{+}}\frac{Gz'\Gamma'^{+}}{\sin\bar{\Theta}}dz'+\epsilon\int_{-h'^{+}}^{\epsilon\zeta'^{+}}\frac{1}{\sin\bar{\Theta}}\left[Gz'\theta'\left(2\cot\bar{\Theta}\Gamma'^{+}+a'\right)+\frac{\partial\phi'^{+}}{\partial t'}\Gamma'^{+}\right]dz'\Bigg\}$$

where the first two integrals are evaluated at $x'=\xi'^{-}$. The last two integrals are evaluated at $x'=\xi'^{+}$, with

$$\Gamma'^{+}=\left(\frac{z'+h'^{+}}{\sin\bar{\Theta}}\right)+a'\cot\bar{\Theta}$$

$$\Gamma'^{-}=\left(\frac{z'+h'^{-}}{\sin\bar{\Theta}}\right)-a'\cot\bar{\Theta} \tag{A.10}$$

being the moment arm of pressure force acting at a given point on the gate walls.

Similar treatment of Taylor expansion about the mean position of the gate surfaces $x'=\bar{\xi}'^{\pm}$ leads to

$$f\left(\mathbf{n},y',t'\right)_{x'=\xi'^{\pm}}=f\left(\bar{\mathbf{n}},y',t'\right)_{x'=\bar{\xi}'^{\pm}}+\frac{\partial f}{\partial\bar{n}}\left(\bar{\mathbf{n}},y',t'\right)_{x'=\bar{\xi}'^{\pm}}\cdot\triangle\mathbf{n}+\cdots \tag{A.11}$$

where f is an arbitrary function, $\mathbf{n}$ is the unit normal vector, $\bar{\mathbf{n}}$ is the mean position of $\mathbf{n}$, and $\triangle\mathbf{n}$ is the small variation of $\mathbf{n}$:

$$\triangle\mathbf{n}=R\triangle\Theta=\Gamma'^{\pm}\cdot\epsilon\theta'$$

thus

$$\frac{\partial}{\partial\bar{n}^{\pm}}=\mp\frac{\partial}{\partial x'}\sin\bar{\Theta}\pm\frac{\partial}{\partial z'}\cos\bar{\Theta} \tag{A.12}$$

After some algebra , we can find from eq. (A.9) that at the order $O(\epsilon^0)$,

$$\begin{aligned}0 &= -\frac{M}{\rho b^3}d'_c\cos\bar{\Theta}+\int_{\Lambda'}dy'\times\\ &\quad\left(\int_{-h'^{-}}^{0}\frac{z'\Gamma'^{-}}{\sin\bar{\Theta}}dz'-\int_{-h'^{+}}^{0}\frac{z'\Gamma'^{+}}{\sin\bar{\Theta}}dz'\right)\end{aligned} \tag{A.13}$$

which is the static equilibrium condition between gravity torque Md'_c and the equilibrium angle $\bar{\Theta}$. The same result can be derived simply by letting $\theta'=0$ and $\phi'=0$

in eq. (A.9). At the next order $O(\epsilon)$, we get

$$\begin{aligned}\frac{I}{\rho b^5}\frac{d^2\theta'}{dt'^2} &= \frac{M}{\rho b^3} G\, d'_c \sin\bar{\Theta}\theta' + \int_{\Lambda'} dy' \times \\ &\left\{ \int_{-h'^-}^{0} \frac{1}{\sin\bar{\Theta}} \left[Gz'\theta' \left(2\cot\bar{\Theta}\Gamma'^- - a' \right) + \frac{\partial \phi'^-}{\partial t'}\Gamma'^- \right] dz' \right. \\ &\left. - \int_{-h'^+}^{0} \frac{1}{\sin\bar{\Theta}} \left[Gz'\theta' \left(2\cot\bar{\Theta}\Gamma'^+ + a' \right) + \frac{\partial \phi'^+}{\partial t'}\Gamma'^+ \right] dz' \right\} \end{aligned} \tag{A.14}$$

A.2 Governing equations

Now we return to physical quantities. As in Section 2.5, Fourier cosine series is used to represent the solution in the half period $0 < y < b$. We then have linearized governing equations of $M_m^{\pm}$:

$$\frac{\partial^2 M_m^{\pm}}{\partial x^2} + \frac{\partial^2 M_m^{\pm}}{\partial z^2} = \left(\frac{m\pi}{b}\right)^2 M_m^{\pm} \tag{A.15}$$

in the fluid,

$$\frac{\partial M_m^{\pm}}{\partial z} - \frac{\omega^2}{g} M_m^{\pm} = 0 \tag{A.16}$$

at $z = 0$,

$$\frac{\partial M_m^{\pm}}{\partial n} = 0 \tag{A.17}$$

at $z = -h^{\pm}(x)$, and

$$\frac{\partial M_m^{\pm}}{\partial \bar{n}^{\pm}} = \mp i\omega\theta^I b_m \left(\frac{z + h^+ \mp a\cos\bar{\Theta}}{\sin\bar{\Theta}} \right) \tag{A.18}$$

at $x = \bar{\xi}^{\pm}(z)$. Consider gate I in $0 < y < b(1-r)$, the dynamic condition of the gate motion eq. (A.14) gives the eigen value condition for ω, the same as eq. (2.50):

$$\omega^2 \left(I + I_a(\omega) \right) = C \tag{A.19}$$

where

$$I_a(\omega) = \frac{i\rho}{\omega\theta^I}\sum_{m=1}^{\infty}\int_0^{(1-r)b}\cos\left(\frac{m\pi y}{b}\right)dy\times \qquad (A.20)$$
$$\left[-\int_{-h^-}^{0} M_m^-\left(\frac{z+h^- - a\cos\bar{\Theta}}{\sin^2\bar{\Theta}}\right)dz + \int_{-h^+}^{0} M_m^+\left(\frac{z+h^+ + a\cos\bar{\Theta}}{\sin^2\bar{\Theta}}\right)dz\right]$$

is the hydrodynamic moment of inertia, and

$$C = -Mgd_c\sin\bar{\Theta} - \rho g\int_0^{(1-r)b}dy\times$$
$$\left\{\int_{-h^-}^{0} z\left[2\cot\bar{\Theta}\left(\frac{z+h^- - a\cos\bar{\Theta}}{\sin^2\bar{\Theta}}\right) - \frac{a}{\sin\bar{\Theta}}\right]dz\right.$$
$$\left. -\int_{-h^+}^{0} z\left[2\cot\bar{\Theta}\left(\frac{z+h^+ + a\cos\bar{\Theta}}{\sin^2\bar{\Theta}}\right) + \frac{a}{\sin\bar{\Theta}}\right]dz\right\} \qquad (A.21)$$

is the total moment due to gravity force and buoyancy, where Mgd_c can be easily derived from

$$Mgd_c\cos\bar{\Theta} = \rho g\int_0^{(1-r)b}dy\times$$
$$\left[\int_{-h^-}^{0} z\left(\frac{z+h^+ + a\cos\bar{\Theta}}{\sin^2\bar{\Theta}}\right)dz - \int_{-h^+}^{0} z\left(\frac{z+h^- - a\cos\bar{\Theta}}{\sin^2\bar{\Theta}}\right)dz\right] \qquad (A.22)$$

For this simplified model where the inclined gates are rectangular boxes, eq.(A.21) and eq.(A.22) can be integrated analytically to get C. For example, when there is no water level difference across the barrier, C is given

$$C = \rho g(1-r)b\times$$
$$\left\{-\int_{-h}^{0} z\left[2\cot\bar{\Theta}\left(\frac{z+h-a\cos\bar{\Theta}}{\sin^2\bar{\Theta}}\right) - \frac{a}{\sin\bar{\Theta}}\right]dz\right.$$
$$\int_{-h}^{0} z\left[2\cot\bar{\Theta}\left(\frac{z+h+a\cos\bar{\Theta}}{\sin^2\bar{\Theta}}\right) + \frac{a}{\sin\bar{\Theta}}\right]dz$$
$$\left. -\left[\int_{-h}^{0} z\left(\frac{z+h+a\cos\bar{\Theta}}{\sin^2\bar{\Theta}}\right)dz - \int_{-h}^{0} z\left(\frac{z+h-a\cos\bar{\Theta}}{\sin^2\bar{\Theta}}\right)dz\right]\frac{\sin\bar{\Theta}}{\cos\bar{\Theta}}\right\}$$
$$= \frac{2\rho gabh^2}{\sin^3\bar{\Theta}}(1-r)\cos^2\bar{\Theta} \qquad (A.23)$$

A.3 Numerical results

For the inclined gate model as shown in Figure A-1, numerical calculations using the hybrid finite element method are performed. The gate is of the same gross dimensions as in the proposed design, *i.e.*, h=15.5 m, b=20 m, and $\bar{\Theta}$=50°, however rectangular-shaped throughout the water depth with thickness of $2a$=4.0 m.

The numerical results are plotted in Figure A-2 with different inclination angles from horizon. The structural inertia I listed in Table 4.2, found by linear interpolation from the recorded data, is also used. The results do not compare well with the prototype tests: the largest error is about 25% when $\bar{\Theta}$=60°. Because the total moment C and the hydrodynamics inertia I_a only depend on the geometry of the gate, the more accurate model is necessary.

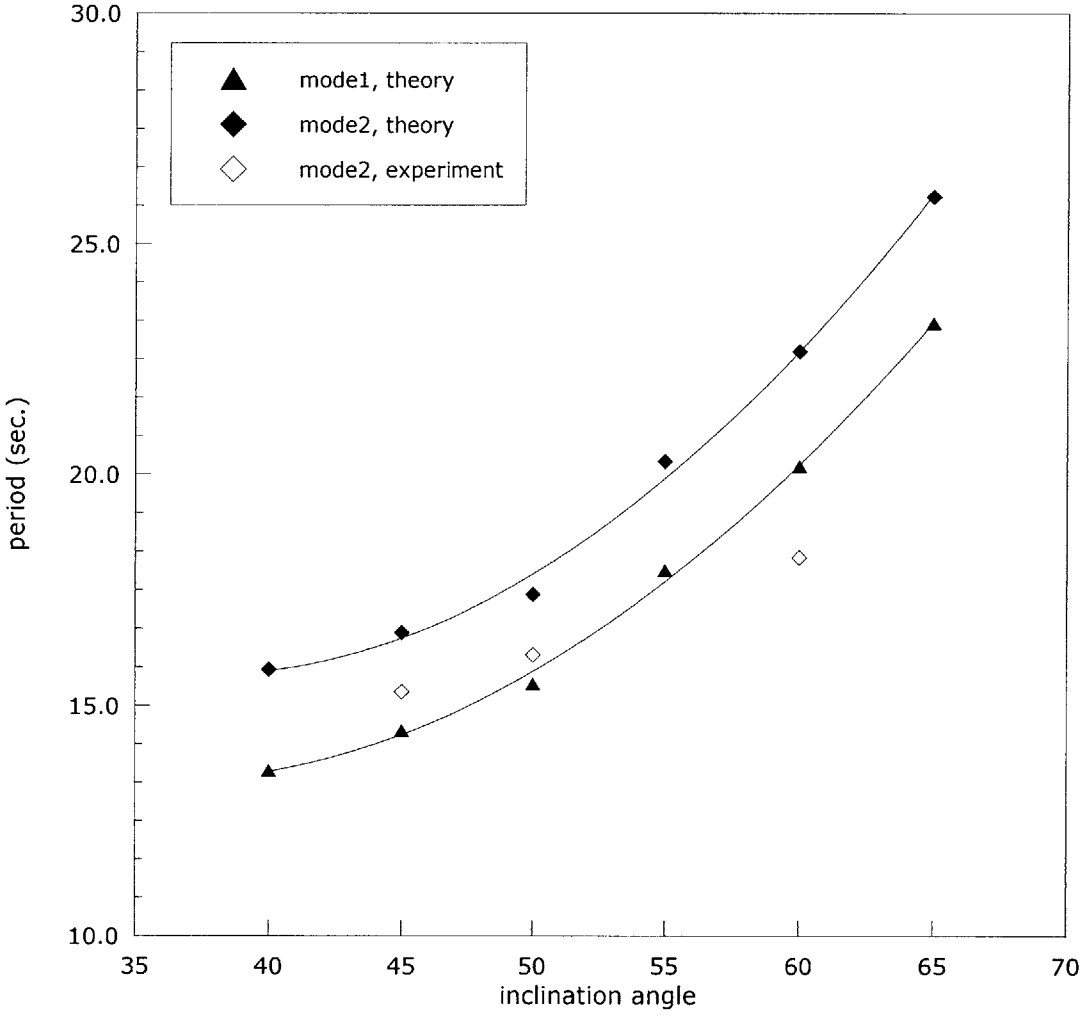

Figure A-2: Natural period of trapped mode for various inclination angles. Using the simplified inclined model.

Appendix B

Fortran program solving the trapped waves

```
C  This program uses Hybrid Finite Element Method to compute the
C  trapped modes around inclined Venice gates.
      PROGRAM VENICE
      REAL ANS,FUNC
      EXTERNAL FUNC
      DIMENSION XYZ(139,2),NCON(218,3),NELEF(50),
     +    NELECP(50),NELECM(50),NELEWP(50),NELEWM(50)
      COMMON/NUMS/ NELE,NNOD,NF,NWP,NWM,NNP,NNM,
     +    NCP,NCM,NCSP,NCSM,NEQT,NBAND
      COMMON/IO/ IREAD,ITERM                                    10
      COMMON/PHYI/ MODE,B,C1,C2,PAI,THETA,M,HP,HM,G,DEN,XCP,XCM
      COMMON/CWIXI/ C,WI,XI

      IREAD=1
      OPEN(UNIT=IREAD,FILE='h155')
      PAI=3.1415926
c  THETA stores (temporarily) the angle of center of gravity
c  relative to the inclination angle.
      THETA=5.2049
      CALL INPUT(XYZ,NCON,NELEF,NELECP,NELECM,NELEWP,NELEWM)    20
      CALL BAND(NCON)
```

```
c  XI is the mass moment of inertia per unit length.
      XI=(1-1./MODE)*B*17.39378e6
      CALL GETC(XYZ,NCON,NELEWP,NELEWM)
      CALL RTSEC(FUNC,0.2,0.4,1.E-5,ANS,
     +    XYZ,NCON,NELEF,NELECP,NELECM,NELEWP,NELEWM)
      WRITE(*,*) ANS,2*PAI/ANS
      STOP
      END

C  Subroutine ASEMK assembles element stiffness matrices into a
C  global stiffness matrix SYSK, which is stored in symm packed form.
      SUBROUTINE ASEMK(XYZ,NCON,SYSK)
      COMPLEX SYSK,ELK
      DIMENSION NCON(NELE,3),XYZ(NNOD,2),SYSK(NEQT,NBAND)
      DIMENSION NR(3),P(3,2),ELK(3,3)
      COMMON/NUMS/ NELE,NNOD,NF,NWP,NWM,NNP,NNM,
     +    NCP,NCM,NCSP,NCSM,NEQT,NBAND

      CALL ERASE(SYSK,NEQT*NBAND*2)
      DO 40 L=1,NELE
        DO 14 J=1,3
          NR(J)=NCON(L,J)
14      CONTINUE
        DO 16 I=1,3
          DO 15 J=1,2
            P(I,J)=XYZ(NR(I),J)
15        CONTINUE
16      CONTINUE
c  Call subroutine SHAPE to calculate element stiffness matrix.
        CALL SHAPE(P,ELK)
        DO 20 I=1,3
          DO 18 J=I,3
            IF(NR(J)-NR(I) .GE. 0) GOTO 17
            LR=NR(I)-NR(J)+1
            SYSK(NR(J),LR)=SYSK(NR(J),LR)+ELK(I,J)
```

```
          GOTO 18
17         LS=NR(J)-NR(I)+1
          SYSK(NR(I),LS)=SYSK(NR(I),LS)+ELK(I,J)                    60
18       CONTINUE
20     CONTINUE
40   CONTINUE
     RETURN
     END


C  Subroutine BAND determines the bandwidth of matrix SYSK.
     SUBROUTINE BAND(NCON)
     DIMENSION NCON(NELE,3)                                        70
     COMMON/NUMS/ NELE,NNOD,NF,NWP,NWM,NNP,NNM,
    +     NCP,NCM,NCSP,NCSM,NEQT,NBAND

     KMAX=0
     DO 10 L=1,NELE
       IMAX=-1
       IMIN=10000
       DO 20 K=1,3
         II=NCON(L,K)
         IMAX=MAX0(IMAX,II)                                        80
         IMIN=MIN0(IMIN,II)
20     CONTINUE
       KMAX=MAX0((IMAX-IMIN+1),KMAX)
10   CONTINUE
     NBAND=MAX0(KMAX,NNP,NNM)
     RETURN
     END


C  Subroutine BKSUBT back-substitutes for solution CX, given         90
C  CA*CX=CB. Solution is retained in CB.
     SUBROUTINE BKSUBT(CA,CB,NEQT,NBAND)
     COMPLEX CA(*),CB(*),C
```

```
      JB=NBAND-1
      DO 10 I=1,NEQT
        C=1.0/CA(I)
        CB(I)=CB(I)*C
        IF(I .EQ. NEQT) GOTO 10
        IB=MIN0(JB,NEQT-I)                                          100
        DO 20 II=1,IB
          INDEX=II*NEQT+I
          CA(INDEX)=CA(INDEX)*C
   20   CONTINUE
   10 CONTINUE
      I1=NEQT-1
      DO 30 I=1,I1
        J=NEQT-I
        IB=MIN0(JB,I)
        DO 40 II=1,IB                                               110
          CB(J)=CB(J)-CA(J+II*NEQT)*CB(II+J)
   40   CONTINUE
   30 CONTINUE
      RETURN
      END


C  Subroutine CROSSK assembles matrix SYSK3 containing cross terms.
      SUBROUTINE CROSSK(NELEC,XYZ,NCON,SYSK3,WK,ALPHA,NN,NCS,IPM,EKC)
      IMPLICIT COMPLEX(S)                                           120
      DIMENSION SYSK3(NN,NCS),NELEC(*),XYZ(NNOD,2),NCON(NELE,3),
     +    WK(NCS),ALPHA(NCS)
      DIMENSION NR(2),P(2),EKC(2,NCS)
      COMMON/NUMS/ NELE,NNOD,NF,NWP,NWM,NNP,NNM,
     +    NCP,NCM,NCSP,NCSM,NEQT,NBAND
      COMMON/PHYI/ MODE,B,C1,C2,PAI,THETA,M,HP,HM,G,DEN,XCP,XCM

c  IPM is the index for either "+"(P) or "-"(M) region.
      IF (IPM .EQ. 1) THEN
```

```
      H=HP                                                              130
      NC=NCP
    ELSE
      H=HM
      NC=NCM
    ENDIF
    CALL ERASE(SYSK3,NN*NCS*2)
    DO 40 L=1,NC
      DO 10 I=1,2
        NR(I)=NCON(NELEC(L),I)
        P(I)=XYZ(NR(I),2)                                               140
10     CONTINUE
      PL=P(2)-P(1)
      PK=WK(1)
      PK1=(H+P(1))*PK
      PK2=(H+P(2))*PK
      COEF=ALPHA(1)/(PK*PK*ABS(PL))
      SH1=SINH(PK1)
      SH2=SINH(PK2)
      CH1=COSH(PK1)
      CH2=COSH(PK2)                                                     150
c Calculate element stiffness matrix for each line segment.
      EKC(1,1)=COEF*(CH2-CH1-PK*PL*SH1)
      EKC(2,1)=COEF*(CH1-CH2+PK*PL*SH2)
      DO 20 J=2,NCS
        PK=WK(J)
        PK1=(H+P(1))*PK
        PK2=(H+P(2))*PK
        COEF=ALPHA(J)/(PK*PK*ABS(PL))
        SN1=SIN(PK1)
        SN2=SIN(PK2)                                                    160
        CS1=COS(PK1)
        CS2=COS(PK2)
c Calculate element stiffness matrix for each line segment.
        EKC(1,J)=COEF*(CS2-CS1+PK*PL*SN1)
        EKC(2,J)=COEF*(CS1-CS2-PK*PL*SN2)
```

```
 20     CONTINUE
c  Assemble to matrix SYSK3.
       DO 30 I=1,2
         DO 3 J=1,NCS
           LR=L+I-1                                                    170
           SYSK3(LR,J)=SYSK3(LR,J)+EKC(I,J)
 3       CONTINUE
 30    CONTINUE
 40  CONTINUE
     RETURN
     END


C  Subroutine DENSE performs static condensation.
     SUBROUTINE DENSE(SYSK,SYSK3P,SYSK3M,SYSK4P,SYSK4M)              180
     IMPLICIT COMPLEX(S)
     DIMENSION SYSK(NNOD,NBAND),SYSK3P(NNP,NCSP),SYSK3M(NNM,NCSM),
    +    SYSK4P(NCSP),SYSK4M(NCSM)
     COMMON/NUMS/ NELE,NNOD,NF,NWP,NWM,NNP,NNM,
    +    NCP,NCM,NCSP,NCSM,NEQT,NBAND

     NN=NNOD-NNP
     DO 28 K=1,NNP
       KK=NN+K
       DO 26 J=1,NNP                                                 190
         KJ=J-K+1
         IF(KJ .LT. 1) GOTO 26
         DO 24 I=1,NCSP
           SYSK(KK,KJ)=SYSK(KK,KJ)-SYSK3P(K,I)*SYSK3P(J,I)/SYSK4P(I)
 24      CONTINUE
 26    CONTINUE
 28  CONTINUE
     DO 38 K=1,NNM
       DO 36 J=1,NNM
         KJ=J-K+1                                                    200
         IF(KJ .LT. 1) GOTO 36
```

```
      DO 34 I=1,NCSM
        SYSK(K,KJ)=SYSK(K,KJ)-SYSK3M(K,I)*SYSK3M(J,I)/SYSK4M(I)
34      CONTINUE
36    CONTINUE
38  CONTINUE
    RETURN
    END


                                                                      210
C  Subroutine DIAGK calculates the diagonal matrix SYSK4.
    SUBROUTINE DIAGK(SYSK4,WK,ALPHA,NCS,IPM)
    IMPLICIT COMPLEX(S)
    DIMENSION SYSK4(NCS),WK(NCS),ALPHA(NCS)
    COMMON/NUMS/ NELE,NNOD,NF,NWP,NWM,NNP,NNM,
   +     NCP,NCM,NCSP,NCSM,NEQT,NBAND
    COMMON/PHYI/ MODE,B,C1,C2,PAI,THETA,M,HP,HM,G,DEN,XCP,XCM

c  IPM is the index for either "+"(P) or "-"(M) region.
    IF (IPM .EQ. 1) THEN                                              220
      H=HP
    ELSE
      H=HM
    ENDIF
    CALL ERASE(SYSK4,NCS*2)
    COEF=-ALPHA(1)
    SYSK4(1)=COEF*(H/2.0+SINH(2.0*WK(1)*H)/(4.0*WK(1)))
    DO 20 J=2,NCS
      COEF=-ALPHA(J)
      SYSK4(J)=COEF*(H/2.0+SIN(2.0*WK(J)*H)/(4.0*WK(J)))              230
20  CONTINUE
    RETURN
    END


C  Subroutine EIGVAL finds required eigenvalues satisfying
C  X*TANH(X)=C, the dispersion relation.
```

```
      SUBROUTINE EIGVAL(N,H,X,Y)
      DIMENSION X(N),Y(N)
      COMMON/PHYI/ MODE,B,C1,C2,PAI,THETA,M,HP,HM,G,DEN,XCP,XCM          240

      TOLR=1.E-5
      C=C1*H
      XJ=C
c  Loop to calculate real root, store in X(1).
 10   XI=XJ
      XJ=C/TANH(XI)
      IF(ABS(XI-XJ) .GT. TOLR) GOTO 10
      X(1)=XJ/H
      Y(1)=SQRT(C2-X(1)*X(1))                                           250
      IF(N .LE. 1) RETURN
c  Loop to calculate imaginery roots, store in X(I).
      DO 30 I=2,N
        XJ=(I-1)*PAI
        DX=XJ
 20     XI=XJ
        XJ=ATAN(-C/XI)+DX
        IF(ABS(XI-XJ) .GT. TOLR) GOTO 20
        X(I)=XJ/H
        Y(I)=SQRT(C2+X(I)*X(I))                                         260
 30   CONTINUE
      RETURN
      END


C  Subroutine ERASE sets consecutive array elements to zero.
      SUBROUTINE ERASE(A,N)
      DIMENSION A(N)

      DO 10 I=1,N                                                       270
        A(I)=0.0
 10   CONTINUE
      RETURN
```

```
      END


C  Subroutine FEM performs Hybrid Finite Element Method for a
C  given frequency W, to get the hydrodynamic moment of inertia WI.
      SUBROUTINE FEM(W,XYZ,NCON,NELEF,NELECP,NELECM,NELEWP,NELEWM)
      IMPLICIT COMPLEX(S)                                              280
      DIMENSION SYSK(139,60),SYSF(139),SYSK3P(5,100),
     +    SYSK3M(5,100),SYSK4P(100),SYSK4M(100)
      DIMENSION WKP(100),WKM(100),ALPHAP(100),ALPHAM(100),
     +    XYZ(NNOD,2),EKC(2,100)
      DIMENSION NCON(NELE,3),NELEF(*),
     +    NELECP(*),NELECM(*),NELEWP(*),NELEWM(*)
      COMMON/NUMS/ NELE,NNOD,NF,NWP,NWM,NNP,NNM,
     +    NCP,NCM,NCSP,NCSM,NEQT,NBAND
      COMMON/IO/ IREAD,ITERM
      COMMON/PHYI/ MODE,B,C1,C2,PAI,THETA,M,HP,HM,G,DEN,XCP,XCM        290
      COMMON/CWIXI/ C,WI,XI

      WI=0.0
c  Loop over modes of Fourier-decomposed potential in y-direction.
      DO 10 M=1,ITERM
        C1=W*W/G
        C2=(M*PAI/B)**2.0
c  Get stiffness matrics SYSK, SYSK3, and SYSK4.
        CALL ASEMK(XYZ,NCON,SYSK)
        CALL SURFK(NELEF,XYZ,NCON,SYSK)                                300
        CALL EIGVAL(NCSP,HP,WKP,ALPHAP)
        CALL EIGVAL(NCSM,HM,WKM,ALPHAM)
        CALL CROSSK(NELECP,XYZ,NCON,SYSK3P,WKP,ALPHAP,NNP,NCSP,1,EKC)
        CALL CROSSK(NELECM,XYZ,NCON,SYSK3M,WKM,ALPHAM,NNM,NCSM,-1,EKC)
        CALL DIAGK(SYSK4P,WKP,ALPHAP,NCSP,1)
        CALL DIAGK(SYSK4M,WKM,ALPHAM,NCSM,-1)
c  Get forcing vector SYSF.
        CALL ERASE(SYSF,2*NEQT)
        CALL LOAD(NELEWP,XYZ,NCON,SYSF,W,1)
```

```
      CALL LOAD(NELEWM,XYZ,NCON,SYSF,W,-1)                              310
c  Static condense the linear system and solve for potentials, store
c  in SYSF.
      CALL DENSE(SYSK,SYSK3P,SYSK3M,SYSK4P,SYSK4M)
      CALL SOLV(SYSK,SYSF,NEQT,NBAND)
      CALL BKSUBT(SYSK,SYSF,NEQT,NBAND)
c  Calculate hydrodynamic moment of inertia WI.
      CALL GETWI(NELEWP,NELEWM,XYZ,NCON,SYSF,W,WI)
 10   CONTINUE
      RETURN
      END                                                               320


C  Subroutine GETC calculates total torque C, consisting of torques
C  due to the weight of the gate and the buoyancy restoring force.
      SUBROUTINE GETC(XYZ,NCON,NELEWP,NELEWM)
      DIMENSION NELEWP(*),NELEWM(*),XYZ(NNOD,2),NCON(NELE,3)
      COMMON/NUMS/ NELE,NNOD,NF,NWP,NWM,NNP,NNM,
     +     NCP,NCM,NCSP,NCSM,NEQT,NBAND
      COMMON/PHYI/ MODE,B,C1,C2,PAI,THETA,M,HP,HM,G,DEN,XCP,XCM
      COMMON/CWIXI/ C,WI,XI                                             330

      CALL GETCR(WTP,CP,XYZ,NCON,NELEWP,1)
      CALL GETCR(WTM,CM,XYZ,NCON,NELEWM,-1)
      WT= G*DEN*(1-1./MODE)*B*(WTM-WTP)
      C = G*DEN*(1-1./MODE)*B*(CP-CM)  - WT*TAN(THETA)
      RETURN
      END


C  Subroutine GETCR uses Gaussian integration to calculate torques   340
C  on either side of the gate.
      SUBROUTINE GETCR(WT,CC,XYZ,NCON,NELEW,IPM)
      DIMENSION NELEW(*),XYZ(NNOD,2),NCON(NELE,3)
      DIMENSION NR(2),X(2),Z(2)
      COMMON/NUMS/ NELE,NNOD,NF,NWP,NWM,NNP,NNM,
```

```
     +    NCP,NCM,NCSP,NCSM,NEQT,NBAND
          COMMON/PHYI/ MODE,B,C1,C2,PAI,THETA,M,HP,HM,G,DEN,XCP,XCM

c  IPM is the index for either "+"(P) or "-"(M) region.
          IF (IPM .EQ. 1) THEN                                          350
c  In z-direction, integrate from -h(0)=-0.5
            H=HP+0.5
            NW=NWP
          ELSE
            H=HM+0.5
            NW=NWM
          ENDIF
          WEIGHT=0.577350269189626
          WT=0.0
          CC=0.0                                                        360
          DO 40 L=1,NW
            DO 10 I=1,2
              NR(I)=NCON(NELEW(L),I)
              X(I)=XYZ(NR(I),1)
              Z(I)=XYZ(NR(I),2)
 10         CONTINUE
            XL=X(1)-X(2)
            ZL=Z(1)-Z(2)
            X0=(X(1)+X(2))/2.
            Z0=(Z(1)+Z(2))/2.                                           370
            X1=X0+WEIGHT*XL/2.
            X2=X0-WEIGHT*XL/2.
            Z1=Z0+WEIGHT*ZL/2.+H
            Z2=Z0-WEIGHT*ZL/2.+H
            FL=SQRT(XL*XL+ZL*ZL)
            AL1=SQRT(X1*X1+Z1*Z1)
            AL2=SQRT(X2*X2+Z2*Z2)
            ATL=ATAN(ZL/XL)
            IF(ATL .LT. 0.0) ATL=ATL+PAI
            AT1=ATAN(Z1/X1)                                             380
            IF(AT1 .LT. 0.0) AT1=AT1+PAI
```

```
      AT2=ATAN(Z2/X2)
      IF(AT2 .LT. 0.0) AT2=AT2+PAI
c  Use COS to find the cross product.
      CROSS1=ABS(COS(ATL-AT1))
      CROSS2=ABS(COS(ATL-AT2))
      IF(1) THEN
        WT=WT+FL/2.*((Z1-H)*AL1*CROSS1+(Z2-H)*AL2*CROSS2)
        CC=CC+FL/2.*( X1  *AL1*CROSS1+  X2  *AL2*CROSS2)
c  Following is the old approach adapting P. Sammarco.                    390
      ELSE
        T=PAI/2-ATL
        TT=TAN(T)
        ST=SIN(T)
        CT=COS(T)
        A=AL1*SIN(ATL-AT1)
        WT=WT+FL/2.*((Z1-H)*(Z1+A*ST)/CT+(Z2-H)*(Z2+A*ST)/CT)
        CC=CC-FL/2.*((Z1-H)*((Z1+A*ST)*2*TT/CT+A)+
     +          (Z2-H)*((Z2+A*ST)*2*TT/CT+A))
      ENDIF                                                              400
 40   CONTINUE
      RETURN
      END


C  Subroutine GETWI calculates hydrodynamic moment of inertia WI.
      SUBROUTINE GETWI(NELEWP,NELEWM,XYZ,NCON,SYSF,W,WI)
      IMPLICIT COMPLEX(S)
      DIMENSION SYSF(NEQT),NELEWP(NWP),NELEWM(NWM)
      DIMENSION NR(2),X(2),Z(2),NCON(NELE,3),XYZ(NNOD,2)                 410
      COMMON/NUMS/ NELE,NNOD,NF,NWP,NWM,NNP,NNM,
     +     NCP,NCM,NCSP,NCSM,NEQT,NBAND
      COMMON/PHYI/ MODE,B,C1,C2,PAI,THETA,M,HP,HM,G,DEN,XCP,XCM

c  Performs the intergration in "+"(P) region.
      SWIP=CMPLX(0.0,0.0)
      DO 40 L=1,NWP
```

```
      DO 10 I=1,2
        NR(I)=NCON(NELEWP(L),I)
        X(I)=XYZ(NR(I),1)                                          420
        Z(I)=XYZ(NR(I),2)
10     CONTINUE
      XP=X(1)+X(2)
c In z-direction, integrate from -h(0)=-0.5
      ZP=Z(1)+Z(2)+2*(HP+0.5)
      XM=X(1)-X(2)
      ZM=Z(1)-Z(2)
      FL=SQRT(XM*XM+ZM*ZM)
      AL=SQRT(XP*XP+ZP*ZP)/2.
      ATM=ATAN(ZM/XM)                                              430
      IF(ATM .LT. 0.0) ATM=ATM+PAI
      ATP=ATAN(ZP/XP)
      IF(ATP .LT. 0.0) ATP=ATP+PAI
c Use COS to find the cross product.
      CROSS=ABS(COS(ATM-ATP))
      SOL=(SYSF(NR(2))+SYSF(NR(1)))*FL*AL*CROSS/2.
      SWIP=SWIP+SOL
40   CONTINUE
c Performs the intergration in "-"(M) region.
     SWIM=CMPLX(0.0,0.0)                                           440
     DO 30 L=1,NWM
       DO 20 I=1,2
         NR(I)=NCON(NELEWM(L),I)
         X(I)=XYZ(NR(I),1)
         Z(I)=XYZ(NR(I),2)
20     CONTINUE
       XP=X(1)+X(2)
       ZP=Z(1)+Z(2)+2*(HM+0.5)
       XM=X(1)-X(2)
       ZM=Z(1)-Z(2)                                                450
       FL=SQRT(XM*XM+ZM*ZM)
       AL=SQRT(XP*XP+ZP*ZP)/2.
       ATM=ATAN(ZM/XM)
```

```
      IF(ATM .LT. 0.0) ATM=ATM+PAI
      ATP=ATAN(ZP/XP)
      IF(ATP .LT. 0.0) ATP=ATP+PAI
c Use COS to find the cross product.
      CROSS=ABS(COS(ATM-ATP))
      SOL=(SYSF(NR(2))+SYSF(NR(1)))*FL*AL*CROSS/2.
      SWIM=SWIM+SOL                                                    460
 30   CONTINUE
     WI=WI+B*REAL((SWIP-SWIM)*CMPLX(0.0,1.0)*DEN
     +    *SIN(M*PAI*(1-1./MODE))/(W*M*PAI))
     RETURN
     END


C Subroutine INPUT reads all physical data and grid system given
C in the input file IREAD.
     SUBROUTINE INPUT(XYZ,NCON,NELEF,NELECP,NELECM,NELEWP,NELEWM)     470
     DIMENSION XYZ(139,2),NCON(218,3),NELEF(*),NELECP(*),NELECM(*),
     +    NELEWP(*),NELEWM(*)
     COMMON/NUMS/ NELE,NNOD,NF,NWP,NWM,NNP,NNM,
     +    NCP,NCM,NCSP,NCSM,NEQT,NBAND
     COMMON/IO/ IREAD,ITERM
     COMMON/PHYI/ MODE,B,C1,C2,PAI,THETA,M,HP,HM,G,DEN,XCP,XCM

     READ(IREAD,900) NNOD,NELE,NF,NCSP,NCSM,
     +    NCP,NCM,NWP,NWM
     NEQT=NNOD                                                        480
     NNP=NCP+1
     NNM=NCM+1
     READ(IREAD,901) ITERM,MODE,THE,B,G,DEN,HP,HM,XCP,XCM
     MODE=MODE+1
c The center of gravity is "THETA" degree relative to the gate.
     THETA=(THE-THETA)*PAI/180.
     B=B*MODE/2
     READ(IREAD,902) (I,XYZ(I,1),XYZ(I,2),L=1,NNOD)
     READ(IREAD,903) (I,NCON(I,1),NCON(I,2),NCON(I,3),L=1,NELE)
```

```
      READ(IREAD,904) (I,NELEF(I),L=1,NF)                                  490
      READ(IREAD,905) (I,NELECP(I),L=1,NCP)
      READ(IREAD,906) (I,NELECM(I),L=1,NCM)
      READ(IREAD,907) (I,NELEWP(I),L=1,NWP)
      READ(IREAD,908) (I,NELEWM(I),L=1,NWM)
  900 FORMAT(5I8/4I8)
  901 FORMAT(2I8/4F8/4F8)
  902 FORMAT(139(/I8,2F16))
  903 FORMAT(218(/4I8))
  904 FORMAT(10(/2I8))
  905 FORMAT(4(/2I8))                                                      500
  906 FORMAT(4(/2I8))
  907 FORMAT(12(/2I8))
  908 FORMAT(10(/2I8))
      CLOSE(UNIT=IREAD)
      RETURN
      END


C Subroutine LOAD determines the forcing vector SYSF.
      SUBROUTINE LOAD(NELEW,XYZ,NCON,SYSF,W,IPM)                           510
      IMPLICIT COMPLEX(S)
      DIMENSION SYSF(NEQT),NELEW(*),XYZ(NNOD,2),NCON(NELE,3)
      DIMENSION NR(2),X(2),Z(2)
      COMMON/NUMS/ NELE,NNOD,NF,NWP,NWM,NNP,NNM,
     +     NCP,NCM,NCSP,NCSM,NEQT,NBAND
      COMMON/PHYI/ MODE,B,C1,C2,PAI,THETA,M,HP,HM,G,DEN,XCP,XCM


c IPM is the index for either "+"(P) or "-"(M) region.
      IF (IPM .EQ. 1) THEN
c In z-direction, integrate from -h(0)=-0.5                                520
        H=HP+0.5
        NW=NWP
      ELSE
        H=HM+0.5
        NW=NWM
```

```
      ENDIF
c  Use Gaussian integration.
      WEIGHT=0.577350269189626
      SBM=CMPLX(0.0,-2.0)*MODE*W*SIN(M*PAI*(1-1./MODE))/(M*PAI)
      DO 40 L=1,NW                                                    530
        DO 10 I=1,2
          NR(I)=NCON(NELEW(L),I)
          X(I)=XYZ(NR(I),1)
          Z(I)=XYZ(NR(I),2)
 10     CONTINUE
        XL=X(1)-X(2)
        ZL=Z(1)-Z(2)
        X0=(X(1)+X(2))/2.
        Z0=(Z(1)+Z(2))/2.
        X1=X0+WEIGHT*XL/2.                                            540
        X2=X0-WEIGHT*XL/2.
        Z1=Z0+WEIGHT*ZL/2.+H
        Z2=Z0-WEIGHT*ZL/2.+H
        FL=SQRT(XL*XL+ZL*ZL)
        AL1=SQRT(X1*X1+Z1*Z1)
        AL2=SQRT(X2*X2+Z2*Z2)
        ATL=ATAN(ZL/XL)
        IF(ATL .LT. 0.0) ATL=ATL+PAI
        AT1=ATAN(Z1/X1)
        IF(AT1 .LT. 0.0) AT1=AT1+PAI                                  550
        AT2=ATAN(Z2/X2)
        IF(AT2 .LT. 0.0) AT2=AT2+PAI
c  Use COS to find the cross product.
        CROSS1=ABS(COS(ATL-AT1))
        CROSS2=ABS(COS(ATL-AT2))
        SYSF(NR(1))=SYSF(NR(1))+IPM*SBM*FL/2.*
     +       (AL1*CROSS1*(X1-X(2))/XL+AL2*CROSS2*(X2-X(2))/XL)
        SYSF(NR(2))=SYSF(NR(2))+IPM*SBM*FL/2.*
     +       (AL1*CROSS1*(X(1)-X1)/XL+AL2*CROSS2*(X(1)-X2)/XL)
 40   CONTINUE                                                         560
      RETURN
```

```
      END


C Subroutine RTSCE(secant method), adapted from Numerical Recipes,
C is used to find the root of eigen function FUNC.
      SUBROUTINE RTSEC(FUNC,X1,X2,XACC,ANS,
     +    XYZ,NCON,NELEF,NELECP,NELECM,NELEWP,NELEWM)
      INTEGER MAXIT
      REAL ANS,X1,X2,XACC,FUNC                                        570
      EXTERNAL FUNC
      PARAMETER (MAXIT=30)
      INTEGER J
      REAL DX,F,FL,SWAP,XL
      DIMENSION XYZ(NNOD,2),NCON(NELE,3),NELEF(*),
     +    NELECP(*),NELECM(*),NELEWP(*),NELEWM(*)
      COMMON/NUMS/ NELE,NNOD,NF,NWP,NWM,NNP,NNM,
     +    NCP,NCM,NCSP,NCSM,NEQT,NBAND
      COMMON/CWIXI/ C,WI,XI
                                                                      580
      FL=FUNC(X1,XYZ,NCON,NELEF,NELECP,NELECM,NELEWP,NELEWM)
      F=FUNC(X2,XYZ,NCON,NELEF,NELECP,NELECM,NELEWP,NELEWM)
      IF(ABS(FL) .LT. ABS(F)) THEN
        ANS=X1
        XL=X2
        SWAP=FL
        FL=F
        F=SWAP
      ELSE
        XL=X1                                                         590
        ANS=X2
      ENDIF
      DO 10 J=1,MAXIT
        DX=(XL-ANS)*F/(F-FL)
        XL=ANS
        FL=F
        ANS=ANS+DX
```

```
      F=FUNC(ANS,XYZ,NCON,NELEF,NELECP,NELECM,NELEWP,NELEWM)
      IF(ABS(DX) .LT. XACC .OR. F .EQ. 0.0) RETURN
   10 CONTINUE                                                        600
      RETURN
      END


C Subroutine SHAPE generates the element stiffness matrices
C in the finite element region.
      SUBROUTINE SHAPE(P,ELK)
      COMPLEX ELK
      DIMENSION P(3,2),ELK(3,3),BB(3),CC(3)
      COMMON/PHYI/ MODE,B,C1,C2,PAI,THETA,M,HP,HM,G,DEN,XCP,XCM          610

      CALL ERASE(ELK,18)
      BB(1)=P(2,2)-P(3,2)
      BB(2)=P(3,2)-P(1,2)
      BB(3)=P(1,2)-P(2,2)
      CC(1)=P(3,1)-P(2,1)
      CC(2)=P(1,1)-P(3,1)
      CC(3)=P(2,1)-P(1,1)
      AREA=ABS(0.5*(BB(1)*CC(2)-BB(2)*CC(1)))
      A4=4.0*AREA                                                      620
      HELM=AREA*AREA*C2/3.0
      ELK(1,1)=(BB(1)*BB(1)+CC(1)*CC(1)+2.0*HELM)/A4
      ELK(1,2)=(BB(1)*BB(2)+CC(1)*CC(2)+    HELM)/A4
      ELK(1,3)=(BB(1)*BB(3)+CC(1)*CC(3)+    HELM)/A4
      ELK(2,2)=(BB(2)*BB(2)+CC(2)*CC(2)+2.0*HELM)/A4
      ELK(2,3)=(BB(2)*BB(3)+CC(2)*CC(3)+    HELM)/A4
      ELK(3,3)=(BB(3)*BB(3)+CC(3)*CC(3)+2.0*HELM)/A4
      RETURN
      END
                                                                       630

C Subroutine SOLV performs Gauss reduction, wehre A is
C stored in symm packed form and B is the forcing vector.
```

```
      SUBROUTINE SOLV(A,B,NEQT,NBAND)
      COMPLEX A(*),B(*),Q,R

      NSOLVE=NEQT-1
      NB=NBAND-1
      JF=NEQT-NB
      DO 10 I=1,NSOLVE                                              640
        Q=1.0/A(I)
        IF(I .GT. JF) NB=NEQT-I
        NB1=NB+1
        DO 20 II=1,NB
          JI=I+II
          R=A(I+II*NEQT)*Q
          B(JI)=B(JI)-R*B(I)
          JJ=NB1-II
          DO 30 IJ=1,JJ
            INDEX1=JI+(IJ-1)*NEQT                                   650
            INDEX2=I+(II+IJ-1)*NEQT
            A(INDEX1)=A(INDEX1)-R*A(INDEX2)
30        CONTINUE
20      CONTINUE
10    CONTINUE
      RETURN
      END


C  Subroutine SURFK calculates free surface contribution and assembles  660
C  into global stiffness matrix SYSK.
      SUBROUTINE SURFK(NELEF,XYZ,NCON,SYSK)
      COMPLEX SYSK,EKS
      DIMENSION NELEF(NF),NCON(NELE,3),XYZ(NNOD,2),SYSK(NEQT,NBAND)
      DIMENSION NR(2),P(2),EKS(2,2)
      COMMON/NUMS/ NELE,NNOD,NF,NWP,NWM,NNP,NNM,
     +     NCP,NCM,NCSP,NCSM,NEQT,NBAND
      COMMON/PHYI/ MODE,B,C1,C2,PAI,THETA,M,HP,HM,G,DEN,XCP,XCM
```

```
      DO 40 L=1,NF                                                    670
        NR(1)=NCON(NELEF(L),1)
        P(1)=XYZ(NR(1),1)
        NR(2)=NCON(NELEF(L),3)
        P(2)=XYZ(NR(2),1)
        PL=ABS(P(2)-P(1))
        EKS(1,1)=-C1*PL/3.0
        EKS(1,2)=-C1*PL/6.0
        EKS(2,2)=-C1*PL/3.0
        DO 30 I=1,2
          DO 3 J=I,2                                                  680
            IF(NR(J)-NR(I) .GE. 0) GOTO 26
            LR=NR(I)-NR(J)+1
            SYSK(NR(J),LR)=SYSK(NR(J),LR)+EKS(I,J)
            GOTO 30
   26       LS=NR(J)-NR(I)+1
            SYSK(NR(I),LS)=SYSK(NR(I),LS)+EKS(I,J)
    3     CONTINUE
   30   CONTINUE
   40 CONTINUE
      RETURN                                                          690
      END


C  Function FUNC is the eigen function for W.
      REAL FUNCTION FUNC(W,XYZ,NCON,NELEF,NELECP,NELECM,NELEWP,NELEWM)
      REAL W,C,XI,WI
      DIMENSION XYZ(NNOD,2),NCON(NELE,3),NELEF(*),
     +    NELECP(*),NELECM(*),NELEWP(*),NELEWM(*)
      COMMON/NUMS/ NELE,NNOD,NF,NWP,NWM,NNP,NNM,
     +    NCP,NCM,NCSP,NCSM,NEQT,NBAND                              700
      COMMON/PHYI/ MODE,B,C1,C2,PAI,THETA,M,HP,HM,G,DEN,XCP,XCM
      COMMON/CWIXI/ C,WI,XI

      CALL FEM(W,XYZ,NCON,NELEF,NELECP,NELECM,NELEWP,NELEWM)
      FUNC=W*W*(XI+WI)-C
```

END

Bibliography

[1] P. Blondequx, G. Seminara, and G. Vittori. Linear response of the gate system for protection of the Venice Lagoon. Note I. Transverse free modes. *Rend. Mat. Acc. Lincei*, A 59:291–298, 1993.

[2] P. Blondequx, G. Seminara, and G. Vittori. Linear response of the gate system for protection of the Venice Lagoon. Note II. Excitation of transverse subharmonic modes. *Rend. Mat. Acc. Lincei*, A 59:299–305, 1993.

[3] H. S. Chen and C. C. Mei. Oscillations and wave forces in an offshore harbor : applications of hybrid finite element method to water-wave scattering. Technical Report 190, M.I.T. Ralph M. Parsons Laboratory for Water Resources and Hydrodynamics, 1974.

[4] D. V. Evans, M. Levitin, and D. Vassiliev. Existence theorems for trapped modes. *J. Fluid Mech.*, 261:21–31, 1994.

[5] D. V. Evans and C. M. Linton. Trapped modes in open channels. *J. Fluid Mech.*, 225:153–175, 1991.

[6] C. M. Linton and D. V. Evans. Hydrodynamic characteristics of bodies in channels. *J. Fluid Mech.*, 252:647–666, 1993.

[7] O. S. Madsen. A three dimensional wave maker, its theory and application. *Journal of Hydraulic Research*, 12(2):205–222, 1974.

[8] C. C. Mei. *The Applied Dynamics of Ocean Surface Waves.* World Scientific, Singapore, 1989.

[9] C. C. Mei, P. Sammarco, E. S. Chan, and C. Procaccini. Subharmonic resonance of proposed storm gates for Venice Lagoon. *Proc. R. Soc. Lond.*, A 444:257–265, 1994.

[10] A. E. Mynett, D. D. Serman, and C. C. Mei. Characteristics of Salter's cam for extracting energy from ocean waves. *Applied Ocean Research*, 1(1):13–20, 1979.

[11] Consorzio Venezia Nuova. Measures for the protection of Venice and its lagoon. Ministry of Public Works, Water Anthority of Venice.

[12] Consorzio Venezia Nuova. Study on the influence of the inclination angle and the gate side shape on gate response: Report on scale model investigation. Technical Report studio 2.2.10, Delft Hydraulics on behalf of Consorzio Venezia Nuova, November 1988.

[13] P. Sammarco. *Theory of subharmonic resonance of strom gates for Venice lagoon.* PhD thesis, Massachusetts Institute of Technology, 1996.

[14] P. Sammarco, H. H. Tran, O. Gottlieb, and C. C. Mei. Subharmonic resonance of Venice gates in waves. Part 2. Sinusoidally modulated incident waves. *J. Fluid Mech.*, 349:327–359, 1997.

[15] P. Sammarco, H. H. Tran, and C. C. Mei. Subharmonic resonance of Venice gates in waves. Part 1. Evolution equation and uniform incident waves. *J. Fluid Mech.*, 349:295–325, 1997.

[16] Pin Tong and John Rossettos. *Finite-element method: basic technique and implementation.* MIT Press, Cambridge, Mass., 1977.

[17] H. H. Tran. Experiments on subharmonic resonance of the Venice lagoon storm gates. Master's thesis, Massachusetts Institute of Technology, 1996.

[18] F. Ursell. Trapping modes in the theory of surface waves. *Proc. Camb. Phil. Soc.*, 47:347–358, 1951.

[19] D. Varisco. Interaction between flap gates and tidal current and waves. *Abstract 23rd Conf. Coastal Engineering, ASCE*, 1992.

[20] G. Vittori. Free and forced oscillations of a gate system as proposed for the protection of Venice Lagoon: the discrete and dissipative model. *Coastal Engineering*, 31:37–58, 1997.

[21] G. Vittori. Oscillating tidal barriers and random waves. *J. Hydraulic Engr.*, pages 406–412, April 1998.

[22] G. Vittori, P. Blondequx, and G. Seminara. Waves of finite amplitude trapped by oscillation gates. *Proc. R. Soc. Lond.*, A 452:791–811, 1996.

[23] Dick K. P. Yue, H. S. Chen, and C. C. Mei. A hybrid element method for calculating three-dimensional water wave scattering. Technical Report 215, M.I.T. Ralph M. Parsons Laboratory for Water Resources and Hydrodynamics, 1976.